Chapter 3

Theory of Ferroalloys Processing

Heikki Jalkanen and Michael Gasik
Aalto University Foundation, Espoo, Finland

Chapter Outline

3.1 GENERAL THEORY OF THE PROCESSES OF FERROALLOYS PRODUCTION

3.1.1 Introduction to Ferroalloys and their Processing

Ferroalloys, by definition, are alloys of two or more metals, of which one is iron. The U.S. Bureau of Mines defines *ferroalloy* as an alloy of iron with at least one other element except carbon. The most conventional elements used in ferroalloys are Mn, Si, Cr, Ca, Al, Ba, Sr, Mg, Ti, V, W, Mo, Nb, REM (including Y, La, and La-group metals), Ta, Zr, Ni, and B. In much smaller quantities, other ferroalloys might be made for specific applications. The

Handbook of Ferroalloys. http://dx.doi.org/10.1016/B978-0-08-097753-9.00003-4

impurities normally considered as harmful (either for the alloy itself or for the steel where this alloy will be applied) are S, P, Cu, Sn, Sb, Bi, As, and so on and gases O, H, and N. The main components of ferroalloys are called leading elements (e.g., manganese is the leading element in ferromanganese). The degree to which the leading element is recovered specifies the technical and economic feasibility and effectiveness of the ferroalloys technology. Analyses and comparisons of the performance of ferroalloys production from raw materials of different composition and method for furnaces in various designs and capacities are usually normalized to basis tons. The *basis ton* of a ferroalloy has a fixed defined content of the leading element. For example, the standard grade ferrosilicon FeSi45 can contain 41% to 47% Si, but the processing parameters and the efficiency are normalized to the 45% Si content. The main classes of commercial ferroalloys are shown in Table 3.1.

The main share of ferroalloys is used in steelmaking for deoxidation and alloying of steels, as well as to modify cast iron, manufacture welding electrodes, and produce compounds as a starting material for the protective coatings for mineral processing. Ferroalloy properties depend largely on the physical and chemical properties of their major elements. Most ferroalloys contain relatively large amounts of iron, which enables the dissolution of the recovered leading element and reduces the activity of the latter, decreases the melting point (or melting range) of many ferroalloys, controls the density, and improves the utilization of the leading elements in steel and alloys deoxidation and alloying. The formation of metallic solutions of a leading element with iron reduces their activity, which favors the change of Gibbs energy for the reduction process.

The quality of ferroalloys includes many parameters besides the variation in chemical composition and size: density, surface conditions, nonmetallic and slag inclusions, and gases (oxygen, hydrogen).

The main indicator of the quality of a ferroalloy is its chemical composition and, above all, the content of the leading element. It is important to have consistency in alloying element amounts in ferroalloys from heat to heat, allowing the manufacture of standard products.

An important feature of the quality of ferroalloys is their size distribution. If the lumps are too large, they might not have time to be dissolved in the liquid steel. If they are too fine, the alloy might oxidize in air or in the slag before acting according to its main function. Also, some fine powders may present a risk of fire or formation of fumes, causing losses of the ferroalloy. Also important are the mechanical properties of ferrous alloys, because they determine the selection of crushing equipment to produce alloys with a predefined grain size.

3.1.1.1 Classification of Ferroalloy Processes by Reductant Type

Reduction by Carbon (Carbothermal Processes)

In these processes, carbon is the main reductant of the metal oxides. The overall reaction can be represented as $MeO_x + yC \rightarrow Me + MeC_z + CO$ (carbides may

TABLE 3.1 Common Classes of Commercial Ferroalloy Types

	Leading Element(s)	Main Products
"Bulk" Ferroalloys		
FeSi, Si	Si	Ferrosilicon (all grades), crystalline silicon
FeMn, SiMn, Mn	Mn, Mn + Si, Mn + N	High-, medium-, low-carbon ferromanganese, silicon manganese, manganese metal, nitrided manganese, manganese, master alloys
FeCr, FeSiCr	Cr, Cr + Si, Cr + N	High-, medium-, low- and ultralow-carbon ferrochrome, charge chrome, ferrosilicochrome, chromium metal, nitrided ferrochrome, and master alloys
"Minor" Ferroalloys		
FeW	W	Ferrotungsten
FeMo	Mo	Ferromolybdenum
FeV	V	Ferrovanadium
Fe(Si)Ca, FeSi(Ba,Mg,Sr)	(Ca,Ba,Sr,Mg) + Si	Silicocalcium (calcium silicon), silicobarium, silicomagnesium, silicostrontium, complex alloys (Fe-Si-Mg-Ca; Si-Ca-Ba-Fe; Si-Ba-Sr and others)
FeNb	Nb, Nb + Ta	Ferroniobium, Ni-Nb, Nb-Ta-Fe; Nb-Ta-Al-Mn-Si-Ti; Nb-Ta-Al
FeTi	Ti	Ferrotitanium, Fe-Si-Ti, Ti-Cr-Al, Ti-Al-Cr-Fe, Ti-Ni
FeB, FeBAl	B, B+Al	Ferroboron, ferroboral and alloys with boron (Ni-B, Cr-V, greynal)
FeAl, FeSiAl	Al, Al + Si	Silico-aluminum, ferro-aluminum, ferrosilicoaluminum, Fe-Al-Mn-Si, Fe-Mn-Al
FeSi-REM	Rare earth metals (sum of REM)	REM-Si; REM-Si-Fe, REM-Al-Si
FeSiZr, FeAlZr	Zr	Ferrosilicon-zirconium, ferroaluminum-zirconium
FeNi, FeCo	Ni, Co, Ni+Co	Ferronickel, ferrocobalt

or may not form depending on the reacting metal and the conditions of the process). One of the major reduction products is carbon monoxide gas, which is removed from the reaction zone, and this provides the irreversibility of the reaction. Carbon can reduce practically all the elements from their oxides at sufficiently high temperatures. The disadvantages of carbon as a reducing agent are mainly the formation of carbides or high-carbon melts and larger required heat input dictating the use of electric arc furnaces of large power.

Reduction by Silicon (Silicothermal Processes)

Silicon reduction of metals from their oxides occurs with the formation of silicon-rich metal melts $MeO_x + Si \rightarrow [Me, Si] + SiO_2$, and in some cases metal silicides might also form if they are stable at the reaction temperatures. Pure silicon is never used as a reductant for economic reasons. Most commonly, silicon is introduced by the same ferroalloy type as being produced but with high silicon content. Thus, silicon reduction of manganese is used with Fe-Mn-Si alloys, and chromium is used for Fe-Cr-Si alloys. These high-silicon alloys are produced separately and used only for reduction purposes. The main advantages of this method are low carbon content in the resulting alloys and exothermic reaction, thus allowing the use of low-power furnaces ($<$10 MVA).

Unlike carbon, silicon oxide is not removed from the furnace and forms a high-silica slag, which upon accumulation decreases the reaction rate and finally stops the process because of the very high activity of silica. To avoid this reaction, fluxes must be added as slag formers (most commonly lime CaO, calcined dolomite [CaO·MgO], or maybe some other products with high basicity).

Silicon as the reducing agent can be used to reduce oxides of elements possessing a higher chemical affinity for oxygen than silicon, if there is an excess of silicon in the melt. Silicon as a reducing agent has some disadvantages: additional use of fluxing agents and difficulty of obtaining low-silicon alloys.

Reduction by Aluminum (Aluminothermal Processes)

Reduction by aluminum proceeds with the reaction $MeO_x + (2x/3)Al \rightarrow Me + (x/3)Al_2O_3$, which is accompanied by a significant exothermal effect. This makes it possible to carry out the process without an external heat supply (out of furnace) or with much less heat versus carbon reduction. During exothermic reactions, a very high temperature might be reached (2400 to 2800 K), which ensures the formation of liquid slag and metal and a good separation of the metal and slag phases at a high rate.

Aluminum is able to reduce a wide range of chemical elements (that have a lower affinity for oxygen than aluminum) and to obtain alloys with very low carbon and silicon, which is essential for getting pure metals (e.g., metallic chromium). The process is relatively simple and requires minor capital costs. It

also could be realized in combination with premelting oxides and fluxes in an electric furnace following out-of-furnace reduction, which can significantly intensify the process and reduce the amount of aluminum required. The high-alumina slags find their utilization in the production of synthetic slags for steel treatment and in high-alumina cements for construction.

The disadvantages of aluminum reduction include the high costs of metallic aluminum, too high viscosity of high-alumina slag (it is difficult to separate metal and slag if the temperature is not high enough), and the possibility of lower metal recovery because of the formation of suboxides of leading metal and aluminates $x\mathrm{MeO}\cdot\mathrm{Al_2O_3}$.

3.1.1.2 Classification of Ferroalloy Processes by Technological Features

Continuous and Batch Processes

Ferroalloy processes are divided into continuous and periodic. Continuous processes are characterized by continuous loading of the charge and periodic (or continuous) slag and ferroalloy tapping. The charge is in the furnace at a certain level throughout the process. The electrodes are immersed in a charge continuously. The furnaces used for these processes usually have high power (>16 MVA) and the reducing agents are carbon materials (coke, char, charcoal, anthracite coal).

Batch processes use a certain amount of charge material for the same heat. The charge loaded into the furnace is completely melt, leading to the reduction of the elements. The products are released periodically (metal and slag tapping), most often at the same time.

Slag and Slag-Less Processes

For the slag-less process, ferroalloys are smelted when the amount of slag formed is small (3% to 5% by weight of the metal), such as in crystalline silicon smelting, and ferrosilicon (FeSi) and ferrosilicochrome (FeSiCr) processing. This slag forms from small quantities of oxides, ores, and concentrates in the coke ash that were not reduced during the heat.

Slag processes, on the other hand, are accompanied by the formation of a considerable amount of slag. The amount of the slag can be 120% to 150% of metal mass smelting of high-carbon ferromanganese (HC FeMn) and ferrosilicomanganese (SiMn) and 200% to 350% for low-carbon ferrochrome (LC FeCr) and manganese metal.

Flux and Fluxless Processes

Smelting of ferroalloys in a batch (periodic) process most often is made by the flux method, although under certain suitable conditions flux-less smelting is feasible. With the fluxing method, the reduction of metal oxides proceeds with the reactions for every reductant type as follows schematically:

$$2MeO \cdot SiO_2 + 2C + CaO = 2Me + 2CO + CaO \cdot SiO_2$$
$$2MeO + Si + CaO = 2Me + CaO \cdot SiO_2$$
$$3MeO + 2Al + CaO = 3Me + CaO \cdot Al_2O_3$$

Introduction of the flux decreases the activity of SiO_2 in the slag, which is accompanied by an increase in the output of recovered metal. Common flux materials contain CaO, MgO, and possibly other components that are able to make up the strongest chemical compounds with reaction products or gangue oxides (SiO_2, Al_2O_3). This also decreases the viscosity of the slag, which leads to a more complete extraction of the leading element and better ferroalloy quality.

In the flux-less method, power consumption is lower and the productivity of the furnace is much higher; however, the degree of recovery of a metal into a ferroalloy decreases. Tapped slag still contains significant amounts of oxides of leading elements and is generally used for the smelting of ferroalloys by carbon reduction—that is, in the second-stage process. The flux-less method can be applied only to high-quality ores and concentrates with low impurities content.

Ferroalloys could also be processed in a secondary metallurgy, using melting of metal and iron scrap or residues from the metallurgical industry, and these processes do not usually involve a substantial reduction part. The raw materials contain oxides, sometimes sulfides or metals (in scrap) of elements other than just the components for a certain ferroalloy to be produced.

The preceding step of any ferroalloy production usually includes sintering, briquetting, or pelletizing raw materials (oxide ores or concentrates) with partial prereduction and partial metallization of iron and some alloying elements prior to the final smelting. The first step of smelting (commonly in a submerged electric arc furnace, electric resistance furnace, or, more seldom, in reverberatory or shaft furnace) is the reduction of the oxides that are still in the solid state before melting. At high temperatures, oxides form liquid slag and, with the progress of the reduction, a metallic phase (melt). The chemical species tend to distribute between the molten ferroalloy melt and the slag in certain proportions. Thus, ferroalloy smelting processes consist of several steps within a wide temperature range, being a combination of step-by-step reduction and formation of molten phases (alloys, slags) and a gas phase (reduction products: carbon monoxide, carbon dioxide, hydrogen, water vapor, gaseous oxides, and other volatile products). The charge being fed into the furnace usually consists of different solid phases (ore lumps or sintered pellets of iron and alloying element, oxide concentrates, slag formers [fluxes], recycled material). Inside the furnace, partially molten charge is placed on the surface of molten slag, which is usually set on the top of molten alloy. There is also a remarkable temperature gradient between the phases present in the furnace and an intensive turbulent mixing of the components, especially near the electrodes.

The basic phenomena of the smelting process are formation and separation of molten ferroalloy and slag. The gangue and the impurities from the ore, which form the slag phase, might be partially reduced and dissolved in the metal alloy. This might be allowable, unless the impurities' concentration exceeds a certain level set by the alloy specification. Impurities could be further removed from the ferroalloy with refinement by special (flux) treatment. The resulting composition of the ferroalloy depends on many thermodynamic and kinetic prerequisites for the formation of molten phases and gas phases by chemical interaction as well as the distribution of raw material constituents between the phases.

All processes in the furnace take place in both macroscopic and atomic-molecular levels. These processes need to have a certain driving force related to the macroscopic and molecular level mechanisms, which control the system inertia (i.e., the rate of the process: rate of chemical reactions, matter and energy transportation). When the equilibrium state is reached, the driving forces of all processes approach zero value and the prerequisites for the advance of processes disappear. The rate of processes depends, on the macroscopic level, on the geometrical and mechanical factors of the process (like the structure and dimensions of the reactor, size and porosity of solid reacting particles like pellets and ore lumps, viscosity, and efficiency of mixing of the liquid and gaseous reacting phases) and in the atomic/molecular level on the resistance of matter transformation processes like chemical reactions and matter transportation processes (diffusion, convection). The driving forces of matter transformation processes are created by affecting the matter *thermally*, conveying heat to the matter (heating) or removing heat (cooling), *mechanically*, increasing or decreasing the pressure, and *chemically*, bringing the matter to be processed in contact with reactive matter leading to a rise of thermodynamic driving forces for chemical transformation and reactions.

3.1.2 Processes in Materials Production

Metals (and materials in general) production, like ferroalloy smelting, is a combination of matter and energy transformation and transportation processes (Table 3.2). A phenomenological classification of major chemical processes at different levels, relevant to ferroalloys production, is shown in Figure 3.1.

From this picture, the major areas of ferroalloys processing theory can be identified as chemical thermodynamics (reduction processes theory, phase formation, phase equilibria), heterogeneous chemical kinetics (the rate of the reactions and phases transformation, different transport processes as regulated by viscosity, electrical conductivity, thermal conductivity, diffusion), and multiphysical phenomena (combined and coupled heat, mass, momentum, and charge transfer in heterogeneous, dynamic media). These areas are briefly described further in this chapter.

TABLE 3.2 Overall Classifications of Generic Processes in Ferroalloys Production

Transformation Phenomena	
Matter	**Energy**
Chemical reaction and phase transitions Phase state change: melting/solidification, evaporation/condensation Dissolution/precipitation Surface processes: adsorption/desorption	Heat release/absorption in matter (phase) transformations Energy conversion in mechanical processes Energy transformation in electromagnetic processes (joule heating, induction heating, reactive losses)
Transportation Phenomena	
Matter	**Energy (Heat)**
Fluid flow transport (convection) Diffusion Osmotic phenomena Flow in porous media	Convective transport with fluid flow Thermal and electrical conduction Electromagnetic radiation

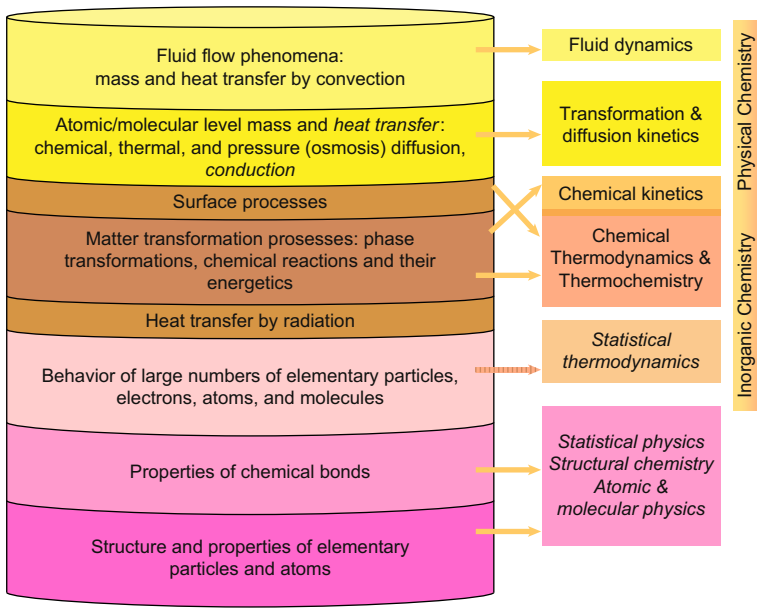

FIGURE 3.1 Schematic presentation of processes from atomic/molecular-level to macroscopic-level phenomena and the theoretical tools used to analyze those phenomena.

3.1.3 Thermodynamics of Pyrometallurgical (High-Temperature Chemical) Processes

3.1.3.1 General Thermodynamic Considerations and Definitions

According to general thermodynamics, the common driving force for any matter and energy transformation process is the tendency to maximize the system entropy S. This means the tendency toward equalization temperature (thermal energy), pressure (mechanical energy), and chemical potentials of all the individual species within the system (reactor, furnace, etc.). Equalization of chemical potentials takes place through matter transformation (reaction within the phase and between the phases) and transportation (diffusion of species from areas of higher chemical potentials to areas of lower chemical potentials). In this context, "chemical potential" should be considered in a more general sense, including purely chemical contributions as well as surface energy, mechanical stress state, and so on if such forces are present.

The equalization of temperature proceeds through conduction, convection, and radiation and equalization of pressure through fluid flow or the deformation of the solid phases. The rate of the total process combination of various matter transformation processes, like in the smelting of ferroalloys, is controlled by the kinetics of chemical transformations (reactions) as well as by the rates of the mentioned matter and energy transportation processes (see Table 3.2 and Fig. 3.1). The rate of chemical reactions, as well as diffusion, normally increases with increasing temperature. The rate of matter transportation by fluid flow depends on the amount of introduced mechanical energy (mixing) and fluidity within the reaction system (viscosity of the liquid/molten phases within the reactor). The rate of matter transportation in solid phases depends on the diffusivity of the species within the phases and the active surface area available (the dispersion degree of the component). The quantitative analysis and modeling of rate phenomena in reaction systems such as ferroalloys smelting processes is a complex and challenging task.

At constant temperature (T) and pressure (P), the general driving force for smelting processes is the tendency to minimize the Gibbs free energy (G) of the system. The Gibbs energy minimization analysis is the normal approach for predicting the tendencies and directions of chemical processes and for defining of the final equilibrium state of the process. Even if the equilibrium state is not reached, it nevertheless reveals to which extent the process might be theoretically implemented.

Thermodynamic and thermal properties of the phases undergoing the transformations are described by the set of principal thermodynamic quantities: entropy (S), enthalpy (H), internal energy (U), Gibbs energy (G), Helmholtz energy (F), and heat capacity (C_p at constant pressure and C_v at constant volume). In spontaneous, uncontrolled processes the entropy tends to increase, and this can be treated as a driving force for matter and energy transformation

and transportation. In controlled processes like most industrial processes where *T*, *P,* or volume (*V*) of the system is kept constant, or stepwise processes along with changing *T/P/V* with a constant amount of matter, the direction of individual matter transformation processes and equilibrium conditions can be analyzed by Gibbs (free) energy *G* at constant temperature and pressure or by Helmholtz (free) energy *F* at constant temperature and volume, respectively. The energy transformations of the system at constant pressure are related to enthalpy *H* and at constant volume (when the system is not doing external work by increasing volume against external pressure) to internal energy, *U*. These quantities are linked to system state variables (*T, P, V,* and *S*) by fundamental differential equations:

$$U\ (\text{internal energy}) : dU\ =\ -PdV + TdS \tag{1}$$

$$H\ (\text{enthalpy}) : dH\ =\ TdS + VdP \tag{2}$$

$$F\ (\text{Helmholtz energy}) :\ dF\ =\ -PdV - SdT \tag{3}$$

$$G\ (\text{Gibbs energy}) : dG\ =\ VdP + SdT \tag{4}$$

The temperature or pressure dependence of the state variables of a single, homogeneous phase (pure element, compound, molten or liquid solution, gas mixture) with constant composition can be obtained from total derivatives of these variables:

$$\begin{aligned} P\ &=\ -\left.\frac{\partial U}{\partial V}\right|_S\ =\ -\ -\left.\frac{\partial F}{\partial V}\right|_T; \qquad T\ =\ \left.\frac{\partial U}{\partial S}\right|_V\ =\ \left.\frac{\partial H}{\partial S}\right|_P; \\ V\ &=\ \left.\frac{\partial H}{\partial P}\right|_S\ =\ \left.\frac{\partial G}{\partial P}\right|_T; \qquad S\ =\ -\left.\frac{\partial F}{\partial T}\right|_V\ =\ \left.\frac{\partial G}{\partial T}\right|_P \end{aligned}. \tag{5}$$

As the material (phase) heat capacity is linked to change of its heat value (thermal energy stored) with temperature, for constant pressure (C_p) or volume (C_v) conditions it might be written as follows:

$$C_P\ =\ \left.\frac{\partial H}{\partial T}\right|_P\ =\ T\left.\frac{\partial S}{\partial T}\right|_P;\ \ C_V\ =\ \left.\frac{\partial U}{\partial T}\right|_V\ =\ T\left.\frac{\partial S}{\partial T}\right|_V. \tag{6}$$

The heat capacity of any material and phase is commonly expressed in the standard polynomial form as a function of temperature,

$$C_P(T)\ =\ A + BT + CT^{-2} + DT^2 + ET^3 + \ldots, \tag{7}$$

where coefficients *A, B, C, D, E,…* are tabulated or included in all existing thermodynamic databases for a number of substances. Temperature dependences of enthalpy and entropy of homogeneous condensed phases are usually written as the sum of integrals of heat capacities of every stable phase state

temperature range plus the sum of the respective enthalpy or entropy of the phase transformation itself (if present; e.g., melting or structure changes):

$$\begin{aligned} H(T) &= H^0_{298} + \sum_{phase} \int_{T_{1,phase}}^{T_{2,phase}} C_P^{phase}(T)dT + \sum_{phase} \left(\Delta H_{phase}\right) \\ S(T) &= S^0_{298} + \sum_{phase} \int_{T_{1,phase}}^{T_{2,phase}} \frac{C_P^{phase}(T)}{T} dT + \sum_{phase} \left(\frac{\Delta H_{phase}}{T_{phase}}\right) \end{aligned} \quad . \tag{8}$$

Here the values with index 298 mean values at the standard reference state (298.15 K and 1 bar pressure), T_1 and T_2 are temperatures of the specific phase stability range, and ΔH_{phase} with T_{phase} are, respectively, the change of enthalpy at the phase transformation and the temperature of this phase transformation. For example, for pure chromium in the temperature range 298 to 1000 K, the heat capacity function (7) in J/mol·K is

$$C_P(T)_{Cr} = 26.906 - 3.784 \cdot 10^{-3} \cdot T - 278500 \cdot T^{-2} + 8.86 \cdot 10^{-3} \cdot T^2$$

and for the range 1000 to 2180 K (until the melting point) it is

$$C_P(T)_{Cr} = 26.911 - 3.79 \cdot 10^{-3} \cdot T - 278010 \cdot T^{-2} + 8.863 \cdot 10^{-3} \cdot T^2$$

(the standard values of H°_{298} and S°_{298} are zero for pure elements by default). When chromium melts, the heat capacity of liquid chromium becomes nearly constant (50 J/mol·K) over 2180 K. However, at the melting point chromium enthalpy is increased by $\Delta H_{Cr} = 21004$ J/mol (latent heat of melting) and entropy by 9.635 J/mol·K. The free Gibbs energy of any phase might be calculated with known enthalpy and entropy values as

$$G(T) = H(T) - T \cdot S(T), \tag{9}$$

where $H(T)$ and $S(T)$ are defined by (8). Additionally, the partial Gibbs energy of the component (known as chemical potential μ_i of this component) is defined as the change of the molar Gibbs energy with an increasing number of moles of this component n_i, keeping T, P, and other component amounts (n_j) constant:

$$\mu_i = \overline{G}_i = \left.\frac{\partial G}{\partial n_i}\right|_{n_j,T,P}. \tag{10}$$

The application of chemical potential is an important part of solution thermodynamics and reactions analysis, as shown in the following discussion. Values of standard states of all elements have been evaluated and presented in a functional form (Dinsdale, 1991).

The common approach to the thermodynamic analysis of chemical processes like pyrometallurgical processes involves constant temperature and pressure; accordingly, the functions used in energy analysis and the analysis of

equilibrium conditions and driving forces of matter transformations are usually enthalpy *H* and Gibbs energy *G*. The equilibrium state of a material system is related to the minimum Gibbs energy of the whole system.

It is important for any thermodynamic analysis to be based on a clear definition of the system and its properties, temperature, pressure, and volume, as well as the amount and quality (elemental composition) of matter. The thermodynamic analysis of the usual metallurgical processes, including the smelting of ferroalloys, is based on an isothermal-isobaric approach (i.e., matter transformations), and their driving forces and equilibrium state are analyzed at constant temperature and pressure. Although temperature in pyrometallurgy is not equal within the furnace or with time (in batch processes), in the great majority of processes the pressure changes are not significant with the advance of the processes (the obvious exception is the vacuum treatment of alloys). This means that a thermodynamic analysis of the processes when based on Gibbs energy minimization should be spatially and timely divided into stages to correctly evaluate the advance of these processes.

In pyrometallurgical processes like reduction and smelting of oxide raw materials for ferroalloys production, the changes of thermodynamic properties of the phases are accompanied by a combination of chemical reactions between the reductant (carbon, silicon, or aluminum) and oxides, formation of slag and molten metal phases, mutual dissolution of oxides and reduced metallic components, phase transformations (melting of solid phases, precipitation of solids from other molten or solid phases as a result of chemical reactions), evaporation of species, and so on. The direction and extent (the equilibrium state) of these processes can be predicted by the combination of the molar Gibbs energy of each phase and the material balance at each level of temperature and pressure. For a process to be thermodynamically possible, the combination of all matter transformations and reactions taking place should lead to a decrease of the total Gibbs energy of the reacting system. By combining enthalpy analyses of the system (all matter transformation processes and energy flows do exchange with the system environment, constituting the heat balance), one will get a comprehensive picture of the process: in which direction the amount and composition of each of the phases present in the process (ferroalloy, slag, furnace gas composition) tend to progress by the individual matter transformation processes at each particular temperature.

Enthalpy analysis connected with the matter transformation processes explains the need of energy to be added to the system (heating) or removed from the system (cooling) when certain temperatures should be achieved in the process environment. Table 3.3 schematically shows the relations between free energy and some important driving forces.

Next, three of the most important applications of thermodynamics in ferroalloys processing are considered in more detail: change of the Gibbs energy with chemical reactions, with formation of solutions, and for describing phase transformations.

TABLE 3.3 Schematic Relations of Gibbs Free Energy and Other Thermodynamic Parameters with Some Important Driving Forces of Different Processes

Type of Process	Driving Force	Remarks
Chemical reactions, phase transformations	$\partial G/\partial \xi\vert_{T,P} < 0$	Change of Gibbs energy with extent of the reaction or transformation progress (ξ)
Species diffusion (molecular/atomic)	$\nabla(\partial G/\partial n_i)_{n_j,T,P} \neq 0$	Gradient of partial Gibbs energy (chemical potential) in space and time
Species diffusion and migration (ionic/charged)	$Z\,\nabla E \neq 0$	Electric field gradient acting on Z-charged species
Surface flow of species	$\nabla\sigma \neq 0$	Nonzero surface energy gradient
Fluid mass flow	$\nabla P \neq 0$	Nonzero pressure gradient, causing velocity **u**
Heat conduction	$\nabla T \neq 0$	Nonzero temperature gradient
Heat convection	$\mathbf{u}\,\rho\,C_P T \neq 0$	Heat flux with fluid at non-zero velocity
Heat radiation	$\Delta T \neq 0$	Nonzero temperature difference between points

3.1.3.2 Thermodynamics of Solutions

Solutions formed by two or more components generally do not preserve their composition if there is a chemical or phase transformation process (which obviously is the goal of alloy processing). In this case, equations (1) through (4) must be complemented by the sum of chemical potentials (10) of all presenting species, $\sum_i n_i d\mu_i$. In the case of equilibrium, the expected change of Gibbs energy (dG) must be zero, thus

$$dG = 0 \rightarrow VdP + SdT + \sum_i n_i d\mu_i = 0, \tag{11}$$

which is known as the Gibbs-Duhem equation. From (11) it immediately follows that at constant temperature and pressure ($dT = dP = 0$), the equilibrium requires no changes in the chemical potentials of the components in all phases.

Upon formation of any solution, the solution free Gibbs energy is not equal to the sum of the free energies of pure constituents because of the increase of mixing entropy. For solutions having k components with n_i moles of every component i, the molar fraction of every component is

$$X_i = \frac{n_i}{\sum_{j=1}^{k} n_j}. \tag{12}$$

The Gibbs energy of 1 mol of the solution is the sum of the Gibbs energies of all of the components, proportional to their molar fractions, plus a contribution from ideal mixing and a contribution from nonideality (called "excess free energy"):

$$\begin{aligned} G^m &= \sum_j X_j G_j^0 + RT \sum_j X_j \ln X_j + \Delta G^{xs} \\ \Delta G^m &= RT \sum_j X_j \ln X_j + \Delta G^{xs} = \Delta H^m - T\Delta S^m, \end{aligned} \tag{13}$$

where $G^\circ{}_j$ is the molar Gibbs energy of pure component j, X_j is molar fraction of the j-component, $R = 8.314$ J/mol·K is the universal gas constant, and ΔG^{xs} is the excess Gibbs energy of mixing. Changes in the enthalpy and entropy of solution formation are defined in the same way as for Gibbs energy (9). The Gibbs energy of ideal mixing describes the effect of dilution of a substance when mixing into the phase without interaction between the components assuming completely statistical random mixing. Any deviations from random mixing of species or a nonzero thermal effect of solution formation make the system nonideal ($\Delta G^{xs} \neq 0$). The excess Gibbs energy of mixing describes the "chemical" interaction between the species in the ($\Delta H^{xs} \neq 0$) phase and deviation from random mixing ($\Delta S^{xs} \neq 0$).

As with equation (10), the chemical potential of a component in the multicomponent solution, expressed in terms of molar fractions, is

$$\mu_i = \left(\frac{\partial G_m}{\partial n_i}\right)_{n_j} = G_m + (1 - X_i)\left(\frac{\partial G_m}{\partial X_i}\right)_{X_j/X_k} - \sum_{j \neq i}^{K-1} X_j \left(\frac{\partial G_m}{\partial X_j}\right)_{X_j/X_k}, \tag{14}$$

which allows the calculation of chemical potential for any cross-section of the compositional space by derivation of Gibbs energy (13). Special care must be taken when selecting proper concentration paths for free energy and chemical potential calculations, because in a multicomponent system they may depend on the integration path. Chemical potential μ_i is an important thermodynamic variable, as it is directly linked with the activity of this component, a_i:

$$a_i(X_i) = \exp\left(\frac{\mu_i(X_i) - \mu_i^0}{RT}\right); \quad \mu_i(X_i) = \mu_i^0 + RT\ln(a_i(X_i)). \tag{15}$$

Activity, or the "corrected concentration" of a component, is a measure of the effectiveness of the component in the solution in respect to its reactions with other components. Raoult made a classical definition of activity, relating activity to the partial pressure of a dissolved component over a solution versus its reference state:

$$a_i(X_i) = P_i(X_i)/P_i^0, \tag{16}$$

where P_i is the partial pressure of this species in the solution and P^0 is the pressure of this substance in the reference state ($a_i^0 = 1$). In Raoultian formalism,

this state is assumed to be pure substance, and many thermodynamic calculations use that by default. The ratio of activity to the real concentration of the component is called the *activity coefficient* $\gamma_i = a_i/X_i$, which is a measure of solution nonideality (in ideal solutions, $\gamma = 1$ in the whole concentration range).

Note that in both definitions of activity (15) and (16), the absolute values depend on the selection of the reference state. The reference state selection is of paramount importance in chemical thermodynamics, as wrong or incompatible states would make all thermodynamic calculations useless.

When the concentration of one component is low enough ("dilute"), a so-called Henrian reference state is assumed whereby the activity coefficient is taken as a constant. This, however, has a limited application, to "dilute" solutions only ($\gamma^{\infty}{}_i = const$ when $X_i \to 0$), and in general the degree of dilution cannot be assigned a numerical value. Thus, a solution seen as a "dilute" one from a practical point of view (such as a few ppm of oxygen in solid chromium) might be nondilute in a Henrian sense (Lupis, 1983; Pelton, 2001).

To obtain the chemical potential (14), the free energy function must be a continuous and differentiable function of the amount of the substance in the solution phase, otherwise the derivation in (14) cannot be performed. The chemical potential and thus activity of the reference state have to be measurable and continuous functions in real solutions.

Historically in metallurgy it was not uncommon to take the reference state as 1 wt. % of the substance in the solvent (in steelmaking, 1% oxygen in liquid iron at 1600°C, for instance, even if such a solution cannot exist). However, as mentioned by some researchers (Hillert, 1998; Kubaschewski and Alcock, 1979; Lupis, 1983), such selections are often confusing and should not be used. Although some handbooks state that the selection of the reference state is a matter of taste and usability, any such selection should not violate basic thermodynamic principles. To determine whether the standard state is correctly defined, the following issues should be taken into account. The activity function of any component must fulfill the following three relations:

$$\left(\frac{\partial \ln a_i}{\partial T}\right)_{P,x_i} = -\frac{\overline{H}_i - \overline{H}_i^0}{RT^2} \tag{17a}$$

$$\left(\frac{\partial \ln a_i}{\partial P}\right)_{T,x_i} = \frac{\overline{V}_i - \overline{V}_i^0}{RT} \tag{17b}$$

$$\left(\frac{\partial \ln a_i}{\partial x_i}\right)_{T,P,x_j/x_k\left(j,k\neq i\right)} > 0. \tag{17c}$$

Two first equations (17a and 17b) are derived from the Clausius-Clapeyron equation. The third equation (17c) follows from (15) and means the activity of any substance in the solution will always increase when it is added to the

system (Gasik, 2001). Thus, every correct reference state must be achievable within the proper concentration range (the solution phase, where it is being sought, must exist). It should always be a state (1) that is achievable by continuously changing the substance concentration while keeping the same solution (phase) structure type, (2) that always has unity value of the activity, and (3) for which its derivatives by temperature (at constant pressure) and by pressure (at constant temperature) are always zero (if they are nonzero, this is not a thermodynamically correct reference state).

For the solutions that do not cover the whole composition range (e.g., in the case of saturation limit), the standard state cannot be chosen as a pure component, because rule (17c) would be violated, and in equations (17a) and (17b) partial enthalpy and partial molar volume respectively would be unobtainable. In such a case (beyond the saturation limit) adding more moles of the compound to the system will not increase its chemical potential in the solution but will only vary the solution fraction (Fig. 3.2). Here the reference state must be chosen at the substance saturation point, when all three relations (17a–c) hold.

Therefore, "hypothetical" states may not generally satisfy the main thermodynamic rules and thus cannot be recommended, as they only cause additional confusion (Kubaschewski and Alcock, 1979). In earlier thermodynamics of metallurgic processes, Wagner formalism with Taylor's series expansion was conventionally used (Lupis, 1983) when the standard state was chosen as 1% wt. of the component even if this solution could not exist. This may cause misleading results when attempting to equilibrate such activities with other phases and should not be used, as emphasized by Kubaschewski and Alcock (1979). Taylor's series expansion is only valid within the vicinity of the differentiation (expansion) point and generally might not be extrapolated over the wider concentration range. Hillert (1998) has also shown that traditional Wagner's expressions for free energy are invalid in respect to the Gibbs-Duhem equation (11) unless a special correction term is added.

Activity and activity coefficient are always functions of temperature, pressure, and composition of the solution phase. The knowledge of the activity

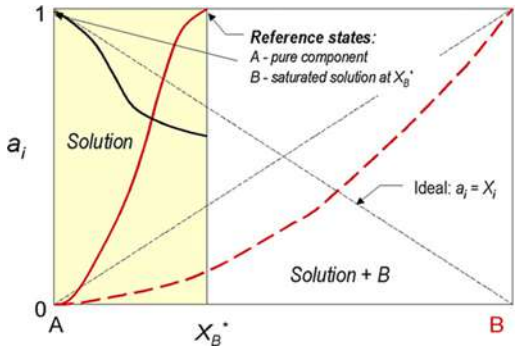

FIGURE 3.2 Activities and reference states in the A-B system with limited solubility.

of a component versus these variables allows one to calculate the resulting mixture and solution composition at some set of environmental variables and to determine favorable process parameters for the smelting or refining processes.

For gaseous mixtures the activity of species is expressed as fugacity, but in most ferroalloys production processes the behavior of gas mixtures is close to ideal (low pressures) and the fugacity is nearly equal to the gas partial pressure. The use of activities is also essential for calculating the system equilibrium when chemical reactions or phase transformations are involved.

3.1.3.3 Thermodynamics of Chemical Reactions

Any chemical reactions between species A_i could be written as

$$v_1A_1 + v_2A_2 + v_3A_3 + \ldots = v_nA_n + v_{n+1}A_{n+1} + v_{n+2}A_{n+2} + \ldots,$$

where v_i refers to stoichiometric coefficients of species. In the short form, the mathematic expression of the reaction is $\sum_i v_iA_i = 0$, where coefficients for the reagents are positive and those for products are negative. The driving force for the reaction is the change of the Gibbs free energy (equations 4 and 9), which might also include changes resulting from the formation of solution (13). Written in terms of chemical potentials, this might be expressed as

$$\begin{aligned}\Delta G_{reac} &= \sum_{products} v_i\mu_i - \sum_{reagents} v_j\mu_j \\ &= \left(\sum_{products} v_i\mu_i^\circ - \sum_{reagents} v_j\mu_j^\circ\right) + RT\left(\sum_{products} v_i\ln a_i - \sum_{reagents} v_j\ln a_j\right),\end{aligned}$$

which can be compactly written as

$$\Delta G_{reac} = \Delta G^0_{reac} + RT\ln\left(\frac{\prod_{products} a_i^{v_i}}{\prod_{reagents} a_j^{v_j}}\right) = \Delta G^0_{reac} + RT\ln K_P. \qquad (18)$$

This equation is known as the acting masses law, connecting free energy change with equilibrium constant K_P, components' activities, and temperature. The reaction proceeds only in the case $\Delta G_{reac} < 0$ and until the ΔG_{reac} reaches zero value. Therefore, in the equilibrium, when no changes are observed in the system, it is experimentally possible to determine components' concentrations and with correct activities calculate the standard Gibbs energy change of the reaction ΔG°. The driving force of all matter transformations—including evaporation, condensation, phase transitions, and precipitation of solids from solution—can be related to Gibbs energies of the phases involved in the process in question.

The standard Gibbs energy of individual formation reaction ΔG° shows the stability of pure compounds, relative tendencies for compound formation, or chemical reactions of species with same reactants. Figure 3.3 presents a diagram

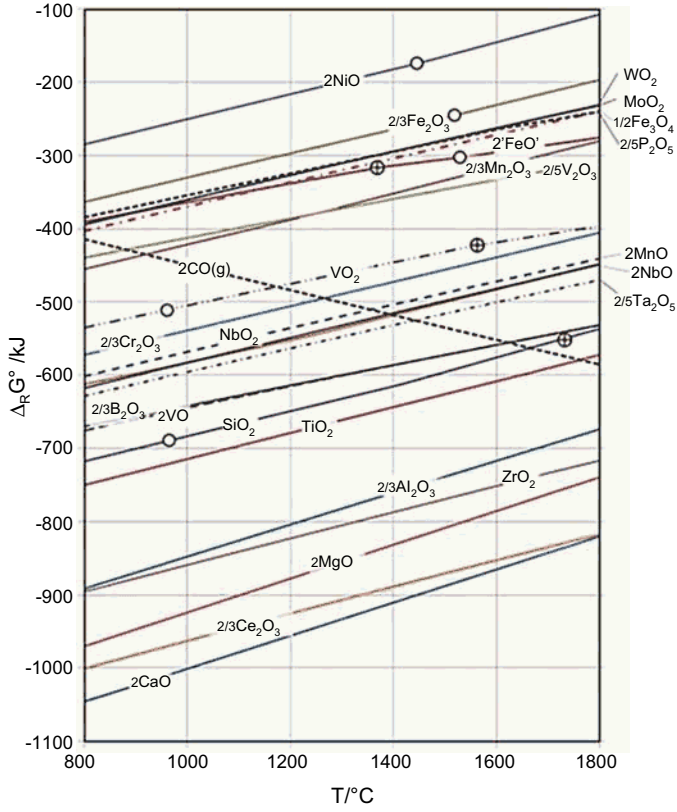

FIGURE 3.3 Ellingham diagram *(ΔG°)* for some oxides corresponding to the reaction of type $2x/y\ Me + O_2(g) = 2/y\ Me_xO_y$ (i.e., per one mole of oxygen O_2. *(Calculated by HSC Chemistry 7.)*

of standard Gibbs energies for the formation of oxides versus temperature (called the Ellingham diagram). The more negative the standard Gibbs energy of reaction is, the stronger the tendency for that reaction and the more stable the formed compound. In general, the element whose oxide has a more negative value of standard Gibbs energy of formation is in principle able to reduce oxides with less negative Gibbs energy of formation.

As Figure 3.3 illustrates, the stability of condensed oxides decreases with increasing temperature with the exception of gaseous carbon monoxide, formed in the carbothermic reduction of oxides, which is the main method used to produce ferroalloys. The increase in the stability of carbon monoxide with temperature means that the efficiency of carbothermic reduction increases with increasing temperature. Carbothermic reduction can be used in principle up to the reduction of titanium if the process is carried out at high temperatures up to 1800°C. The information in Figure 3.3 reveals that the most easily reducible oxide of common ferroalloy elements is nickel oxide and the most stable one is

cerium oxide. However, one has to keep in mind that this diagram (as do similar ones) assumes activities of all components equal to unity (pure phases) and does not take into account possible gaseous suboxides formation (e.g., SiO, Al_2O, AlO) or carbides (TiC, Cr_3C_2, etc.). When a reducible element forms a solution (e.g., with iron), its activity drops and the theoretical reduction temperature (when $\Delta G^\circ = 0$) decreases. This is one of the reasons why it is possible to produce many metals in the form of ferroalloys, but not as pure elements (Al, Ca, Mg, Zr, Ti, REM, etc.).

For example, let's consider reduction of silicon by carbon:

$$SiO_2 + 2C = Si + 2CO_{(gas)}, \quad \Delta G^\circ_{SiO_2} = 494711 - 355.26 \cdot T, \ \mathrm{J/mol}.$$

The analysis shows that the temperature when $\Delta G^\circ{}_{SiO_2}$ reaches zero value is 1665°C. It shows when the reduction starts if all silica, carbon, and silicon are pure phases and the gas is only carbon monoxide at 1 bar pressure (i.e., the reaction equilibrium constant $K_P = 1$). To determine what happens if one of these conditions does not hold, let's write a total Gibbs energy (18) for this reaction:

$$\begin{aligned} \Delta G_{SiO_2} &= \Delta G^0_{SiO_2} + RT\ln\left(\frac{P^2_{CO}\cdot a_{Si}}{a_{SiO_2}\cdot a_C}\right) \\ &= 494711 - 355.26\cdot T + 8.314\cdot T\ln\left(\frac{P^2_{CO}\cdot a_{Si}}{a_{SiO_2}\cdot a_C}\right). \end{aligned} \tag{19}$$

Suppose that the process uses pure carbon reductant ($a_C = 1$) and the gas phase consists of only CO ($P_{CO} = 1$). In this case, the temperature of the reduction is determined by $\Delta G_{SiO_2} = 0$, which now depends on the a_{Si}/a_{SiO_2} ratio (Table 3.4).

As follows from Table 3.4 and equation (19), it is beneficial to decrease the activity of the reduced element (silicon) by, for example, forming a ferroalloy melt and increasing the activity of the oxide being reduced. This rule of thumb applies to all metallurgical processes, including ferroalloys.

Other common reductants used in the metallothermic reduction of ferroalloys (silicon and aluminum) are more powerful in reducing ferroalloy

TABLE 3.4 Dependence of the Starting Reduction Temperature for Silica Reduction by Carbon (19) from the Activities of Silicon and Silica

Activity of SiO_2	Activity of Si	Ratio a_{Si}/a_{SiO_2}	Calculated Temperature of Reduction, °C
1	1	1	1665
1	0.5	0.5	1635
1	0.1	0.1	1566
0.5	0.1	0.2	1595

components (Fe, Ni, W, Mo, Mn, Nb, Ta, V, B, Si, Ti, Zr, and Ce) than carbon because they have higher negative Gibbs energy values of the reaction. Figure 3.4 shows the difference in reduction efficiency among carbon, silicon, and aluminum in relation to some oxides of common ferroalloy elements. For the elements forming the most stable oxides (like zirconium and cerium), the more effective reductants are magnesium and calcium, as Figures 3.3 and 3.4 show. Metallothermic reduction is applied also when the low-carbon ferroalloys are required, even when carbothermic reduction is effective enough.

In considering the data shown in Figure 3.4, one has to keep in mind that these Gibbs energy values are standard ones (i.e., for pure phases only). For instance, if the reduction of ZrO_2 by Si has too much positive free energy to proceed, it does not mean that a reduction of zirconium is impossible at low zirconium concentrations and realistic temperatures. At 1600°C, $K_P = 1.265 \cdot 10^{-5}$ for the reaction $ZrO_2 + Si = SiO_2 + Zr$, so with pure silicon, silica, and zirconia the reaction will be still possible if $a_{Zr} < K_P$. In the actual process, however, all the elements form solutions, so the effect of changes to activities will be more complex and sometimes not straightforward because there might be competitive reactions.

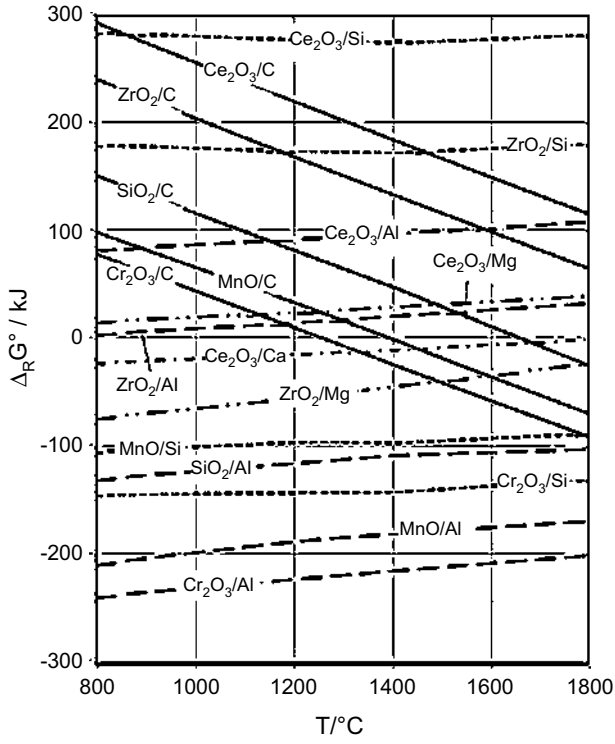

FIGURE 3.4 Comparison of standard Gibbs energies of reduction reactions of some oxides by Al, Si, and C per one mole of reductant. *(Calculated by HSC Chemistry 7.)*

In the carbothermic smelting of ferroalloys there are some undesired side reactions, like the evaporation of species in the form of volatile oxides and solid carbides. The latter phenomenon is not necessarily harmful if high carbon content in the alloy is permissible. Some standard Gibbs energies for metal carbides formation are presented in Figure 3.5. This Ellingham diagram for the formation of carbides shows that the tendency for the formation (precipitation) of carbides during the carbothermic smelting of ferroalloys increases in the following order: Fe (the least stable), Mn, Al, Si, B, Mo, Ce, V, Cr, Ti, and Ta (the most stable).

Chemical reactions tend to proceed at constant temperature and pressure in a reaction system in so far as they lead to the decrease of the system's Gibbs energy (i.e., when an equilibrium state has been reached). Consider, as another example, the formation of ferronickel by the reduction of wüstite ('FeO') and nickel monoxide (NiO):

$$\text{'FeO'} + \text{CO(g)} = \text{Fe} + \text{CO}_2(g), \Delta G_{FeO} \Delta G^0_{FeO} + RT \ln \frac{a_{Fe}\, P_{CO_2}}{a_{FeO} P_{CO}} \quad (20)$$

$$\text{NiO} + \text{CO(g)} = \text{Ni(l)} + \text{CO}_2\text{(g)} \;\; \Delta G_{NiO} = \Delta G^0_{NiO} + RT \ln \frac{a_{Ni}\;\; P_{CO_2}}{a_{NiO}\;\; P_{CO}}. \quad (21)$$

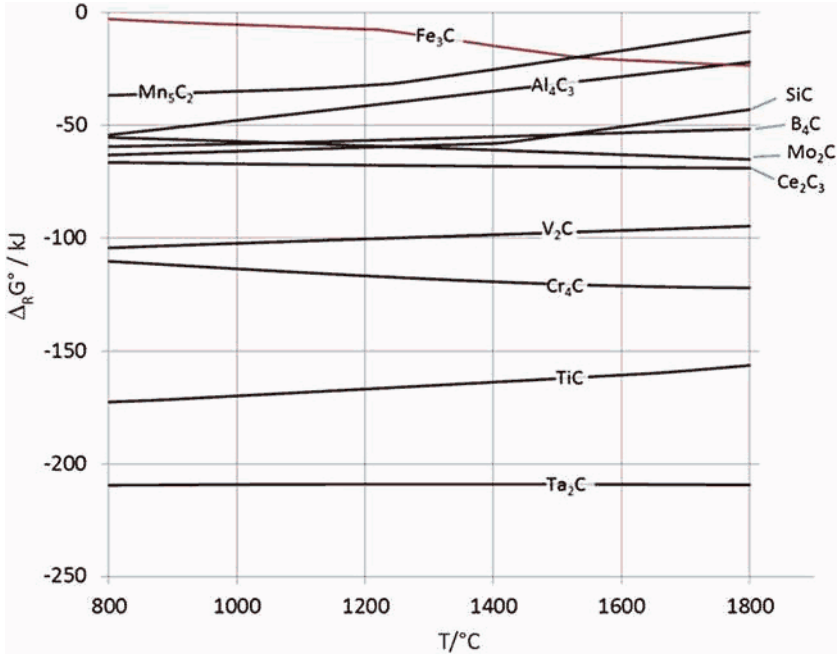

FIGURE 3.5 Standard Gibbs energies of formation of some carbides per one mole of carbon. *(Calculated by HSC Chemistry 7.)*

Figure 3.6 presents the change of Gibbs energy at 1600°C under atmospheric pressure with the progress of the reactions for the system, which has only iron oxide; Figure 3.7 presents the change for the system with an equimolar 1:1 ratio of 'FeO' and NiO. In the second example, the oxides form a molten mixture and the reduction products form a binary alloy (ferronickel). At high temperatures both 'FeO'-NiO and Fe-Ni binary systems are close to ideal solutions—that is, the activities of these components are close to their mole fractions. The chemical reactions tend to proceed in so far as the derivative of system Gibbs energy in relation to reaction extent (∂G/∂ξ) is negative until it reaches the zero value where the Gibbs energy minimum has been reached.

Figures 3.6 and 3.7 show that the total Gibbs energy change might be lower than the standard value because of the formation of solutions and changes in the components' activities. In Figure 3.7 this requires a three-dimensional representation, as there are more degrees of freedom in the system. The minimum of the free energy is reached, resulting in an alloy with 0.78 mol Ni and 0.025 mol

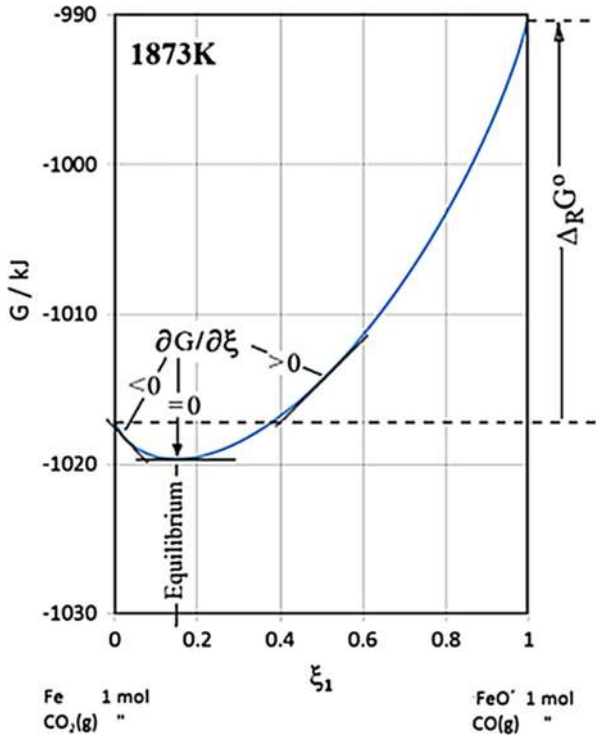

FIGURE 3.6 Gibbs energy of a reaction system '*FeO*'+ *CO(g)* as a function of the reaction progress (reaction extent ξ) and the driving force of the reduction reaction, the first derivative of Gibbs energy with reaction extent ξ. *(Calculated by HSC Chemistry 7.)*

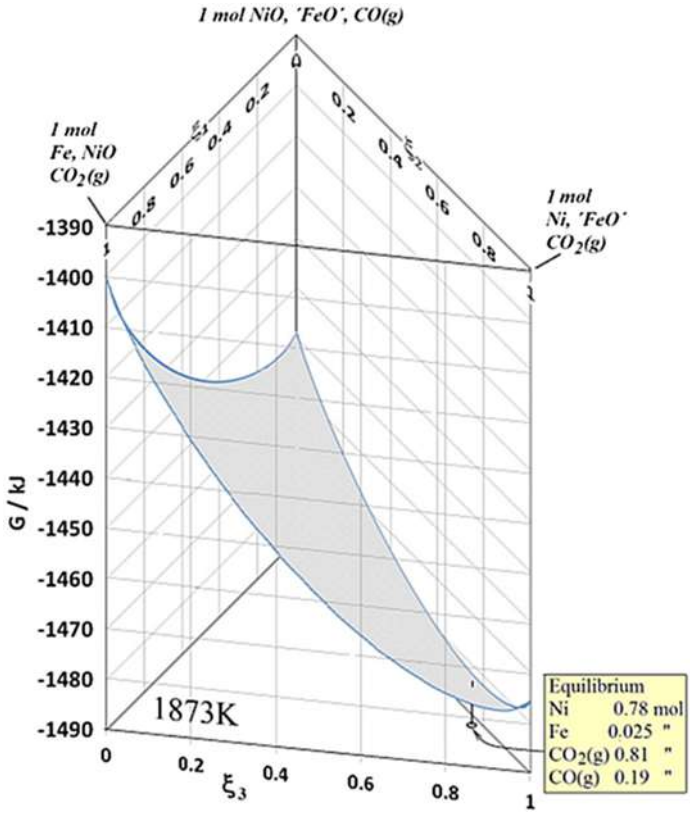

FIGURE 3.7 Gibbs energy surface of a reaction system with initial composition 'FeO' + NiO + CO(g) as a function of the reaction extent of independent reduction reactions 'FeO'+ CO(g) = Fe + CO_2(g) and NiO + CO(g) = Ni + CO_2(g). The third reaction, Ni + 'FeO' = Fe + NiO, is not independent but is a sum of 'FeO' reduction and NiO oxidation reactions. $\Delta_R G^\circ(1873K) = 27.1$ kJ/mol for 'FeO 'and −48.1 kJ/mol for NiO reduction. *(Calculated by HSC Chemistry 7.)*

Fe (~96.8% Ni mol), although the starting nickel concentration was 50% mol. The difference shows that in this case nickel (rather than iron) is preferentially reduced, leading to Ni-rich alloy formation.

The rate of the reactions depends on the kinetics of the chemical interaction and mass transfer in every specific case. If there are several reactions using the same reactants, such as in the system consisting of wüstite ('FeO') and nickel oxide, and the rates of the reactions are different, one reaction can pass the equilibrium state, but with time the system will return to the equilibrium state by opposing reactions with gaseous and condensed reactants. So if the reduction of nickel oxide is faster (in the second example) and its reduction passes the total equilibrium composition, the equilibrium state tends to be approached by a backward reaction (NiO) $+[Fe]_{alloy} = [Ni]_{alloy} +$ ('FeO').

Therefore, besides the standard Gibbs energy of reaction, changes of elements and species activities (the formation of solutions) control the driving force of the process and the equilibrium state of chemical interaction. Figure 3.8 shows the progress of equilibrium reduction of iron chromite $FeCr_2O_4$ as a function of carbon addition at 1600°C (calculated using FactSage 6.2 databases) with the solution model for liquid iron-based solution. The first reduction reaction is $FeCr_2O_4 + C(s) \rightarrow Fe(l) + CO + Cr_2O_3$ and the second one (progressing significantly when the first one is practically finished) is $Cr_2O_3 + 3C \rightarrow 2[Cr]_{FeCr} + 3CO$.

So the liquid iron forms first, and then it dissolves reduced chromium lowering its activity and assisting the reduction process. According to information in the database for Fe alloys in FactSage 6.2, the activity coefficient of Cr in the Fe-Cr-C alloy is about 0.8 to 0.95 and that of C is about 0.1 to 0.5, increasing with each increasing degree of reduction. When chromium oxide is completely reduced and oxygen potential in the reaction system is reduced to a certain, sufficiently low level, there is a tendency for chromium carbide to form (the next reaction).

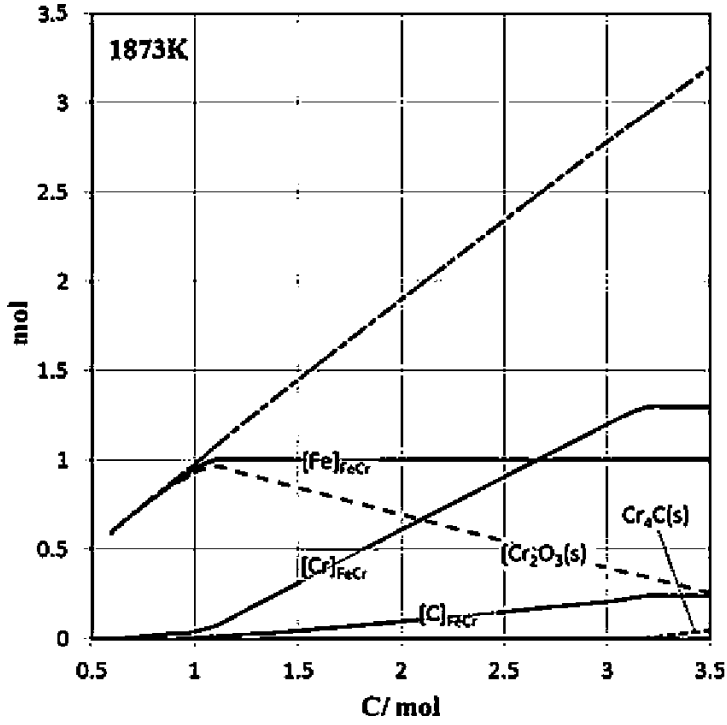

FIGURE 3.8 The progress of equilibrium reduction of one mole of chromite, $FeCr_2O_4$, by carbon and the formation of ferrochromium (FeCr) as a function of carbon addition. *(Calculated by FactSage 6.2.)*

The reduction of oxides by CO formed during primary carbothermic reduction (by carbon) is also possible depending on the stability of oxide and the activity of reduced components in molten ferroalloy, although this process plays a certain role only for metals with less stable oxides (NiO, MoO_2, WO_2, 'FeO'). The role of carbon monoxide in the carbothermic reduction could be important as the secondary reductant, especially as the kinetic prerequisites for gaseous reduction are better because of the higher mobility of reductant than in solid-solid, solid-molten, or molten-molten reduction—carbon does not melt, even at high temperatures, not to mention its evaporation. Even if carbon monoxide is not as such an effective reductant for most ferroalloy component oxides, the back reduction of carbon dioxide $CO_2 + C(s) \rightarrow 2CO$, formed in the secondary reduction by carbon monoxide (chromium oxide reduction, for example) $Cr_2O_3 + 3CO \rightarrow 2[Cr]_{FeCr} + 3CO_2$, will keep the partial pressure of carbon dioxide low in the reaction environment and enables the reduction of even stable oxides by carbon monoxide (Gasik, 2001).

Thermodynamic calculations concerning the advance of individual reactions and final equilibrium state in metallurgical processes such as ferroalloys melting offer important information about the behavior of the reaction environment under various stages of the process, important for ruling and running the process, even when the final equilibrium state in the actual process has not been reached. Calculations of the equilibrium state of complex high-temperature processes like the various stages of ferroalloy smelting are hard to determine because of the complexity of the reaction system—a series of reactants and uneven conditions like temperature and charge composition at various locations in the reactor. In ferroalloys smelting based on lumpy ore or pelletized concentrates and carbon from coal with impurities as reductant, complex solid and molten phases with often remarkable amounts of various components, not only the oxides of iron and desired alloy element in the charge and formed alloy, can contain a number of auxiliary components.

There are a series of commercial programs for thermodynamic calculations, even for complex reaction environments like those in ferroalloy smelting, with a series of models for both metallic and nonmetallic solution phases. Typical examples are HSC Chemistry (www.outotec.com/HSC), FACTSage (www.factsage.com), ThermoCalc (www.thermocalc.se), Pandat (www.computherm.com/pandat.html), and MatCalc (matcalc.tuwien.ac.at). Modern thermodynamic databases are organized for automated data retrieval, so there is less use for tabulating standard Gibbs energy values or activity functions.

3.1.3.4 Equilibrium Phase Diagrams

In the development of new and the improvement of existing technological processes of ferroalloys production, the phase equilibria data in binary, ternary, and more complex metal, oxide, nitride, silicide, and carbide systems are of great importance. Study of the position of the boundary lines, equilibrium

concentration fields of the phases, and their physical transformation ranges is crucial for alloy compositions and for the determination of optimal processing parameters. Many phase equilibria diagrams are calculated with thermodynamic databases and the support of experimental data by thermal analysis. Phase diagrams of elements help to explain why the formation of only certain grade compositions of ferroalloys is beneficial, why the slags formed should have proper composition, and how the process parameters should be adjusted in relation to changes in chemical composition and temperature.

This is a brief outline of only the phase diagram types and their peculiarities; the reader is advised to consult specialist literature related to the theory of phase equilibria and the CALPHAD (CALculation of PHAse Diagrams) method in general (Dinsdale, 1991; Hillert, 1998; Kubaschewski and Alcock, 1979; Pelton, 2001). It is a well-known procedure based on the concept of deriving the thermodynamic functions of a system from all available experimental data (Dinsdale, 1991; Saunders and Miodownik, 1998). The thermodynamic functions are expressed as polynomials of temperature, and the numerical values of the polynomial coefficients are obtained using optimization techniques (Pelton, 1988). The Gibbs energies of pure elements with respect to temperature $G_i^0(T)$ are represented by $G_i^0(T) = a + bT + cT\ln T + dT^2 + e/T + fT^3 + iT^4 + jT^7 + k/T^9$, as referred to the constant enthalpy values of the Standard Element Reference (SER) H_i^{SER} at 298.15 K and 1 bar (Dinsdale, 1991). The solution phases (liquid, solid solutions) are described by substitutional or interstitial solution models, where the Gibbs energy of the phase is given by (13) and the excess Gibbs energy G_i^{xs} is expressed in different forms.

For example, in the binary Fe-Cr system, four phases may formally exist. The liquid phase has only one sublattice (no miscibility gap) with Cr and Fe, whereas the BCC phase has two sublattices (1:3 ratio; Fig. 3.9) with chromium and iron in one and vacancies in the other, $(Cr,Fe)(Va)_3$. The iron-rich FCC phase also has two sublattices, but with the equal ratio (Cr,Fe)(Va). The most complex structure has sigma-phase CrFe, which thermodynamic description requires three sublattices $(Fe)_8(Cr)_4(Fe,Cr)_{18}$.

For a simple substitutional solution (only one lattice site with random occupation, e.g., liquid phase) for the excess Gibbs terms, using the Redlich-Kister-Muggianu polynomial, one obtains

$$G_m^{xs} = \sum_i \sum_{j<i} X_i X_j \sum_{v=0}^{v_{\max}} {}^{v}L_{ij}\left(X_i - X_j\right)^v + \sum_i \sum_{j<i} \sum_{k<j} \frac{X_i X_j X_k}{X_i + X_j + X_k}\left(X_i L_i^{(ijk)} + X_j L_j^{(ijk)} + X_k L_k^{(ijk)}\right), \quad (22)$$

where L_{ij} are respective binary and ternary temperature-dependent interaction parameters. For example, the expression for excess Gibbs energy for the liquid Fe-Cr phase might be written as $G_{LIQ}^{xs} = X_{Fe}X_{Cr}({}^0L_{FeCr} + {}^1L_{FeCr}(X_{Fe} - X_{Cr}))$.

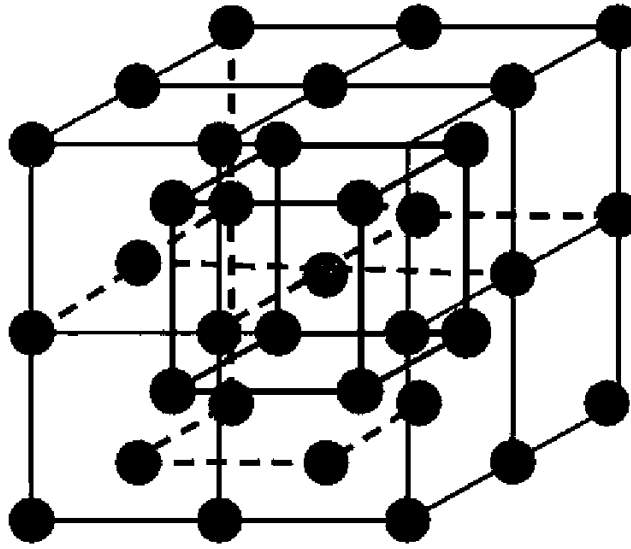

FIGURE 3.9 The model of two sublattices in the BCC Fe-Cr solid solution.

Numerical values of interaction parameters are retrieved from thermodynamic databases during calculations.

As all the ferroalloys systems are rather complex, involving many species and elements, the easiest way to start is to examine the binary phase diagrams of major components, moving further to cross sections of ternary and higher systems and adding more and more components. The hypothetical complex phase equilibrium diagram A-B shown in Figure 3.10 summarizes most possible phase transitions and transformation reactions, explained in Table 3.5 (Gasik et al., 2009).

Some of the phase diagrams are shown schematically in Figures 3.11 through 3.13. The simplest phase diagrams appear when A and B components have full mutual solubility in solid and liquid states (Fig. 3.11). This is typical for isomorphic systems and for components with very close properties. Figure 3.12 shows the eutectic system, where A and B are partially soluble in the solid state but completely soluble in liquid. This leads to a separation of the solid solutions α and ß upon cooling, finishing with spontaneous eutectic solidification below eutectic temperature.

The eutectoid system is similar to that described earlier, but here A and B form several solid solutions, where in the high-temperature one (γ-phase) they have complete solubility. Upon cooling, this phase undergoes eutectoid transformation with a mechanism similar to that used for the eutectic one but without the liquid phase. A well-known system is iron-carbon with eutectoid temperature ~738°C at 0.8%C, which is important for the heat treatment of steels. Many systems in ferroalloys production have this kind of transformation.

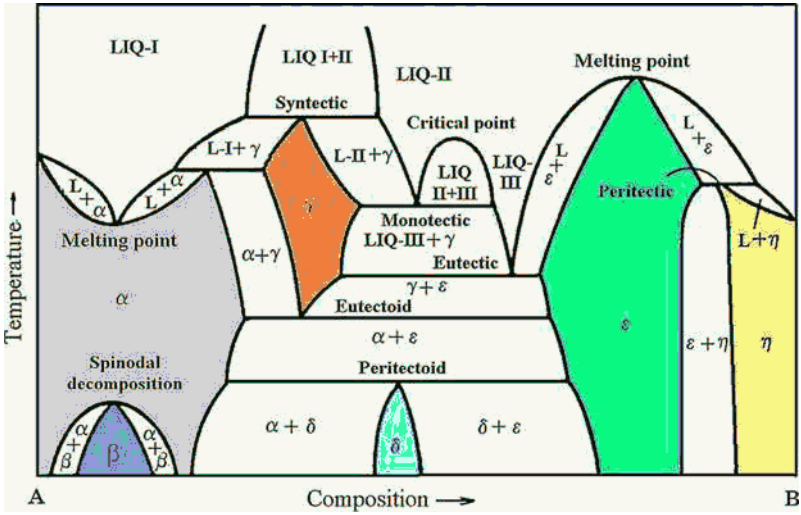

FIGURE 3.10 The hypothetical phase equilibria diagram showing possible phase transformations in a binary system. Areas of stability of homogeneous solid phases are shaded. *(From Gasik et al., 2009.)*

TABLE 3.5 General Classification of Different Phase Transformations (see Fig. 3.10)

Name	Reaction Type (Examples in Fig. 3.10)
Eutectic Type	
Eutectic	$L_{III} \leftrightarrow \gamma + \varepsilon$
Eutectoid	$\gamma \leftrightarrow \alpha + \varepsilon$
Monotectic	$L_{II} \leftrightarrow \gamma + L_{III}$
Monotectoid	$\gamma \leftrightarrow \gamma_1 + \beta$ (not shown in Fig. 3.10)
Catatectic	$\gamma \leftrightarrow L_I + \beta$ (not shown in Fig. 3.10)
Peritectic Type	
Peritectic	$L_I + \gamma \leftrightarrow \alpha$; $L + \varepsilon \leftrightarrow \eta$
Peritectoid	$\alpha + \varepsilon \leftrightarrow \delta$
Syntectic	$L_I + L_{II} \leftrightarrow \gamma$
Other	
Spinodal decomposition	$\alpha \leftrightarrow \beta + \alpha_I/\alpha_{II}$
Critical point	$L_I + L_{II} \leftrightarrow L$; $L_{III} + L_{II} \leftrightarrow L$

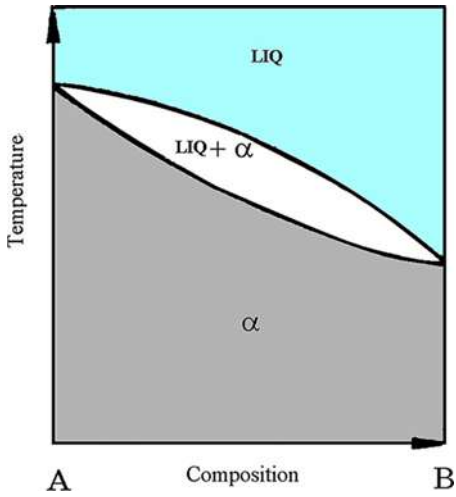

FIGURE 3.11 Equilibrium phase diagram showing complete solubility in solid and liquid states.

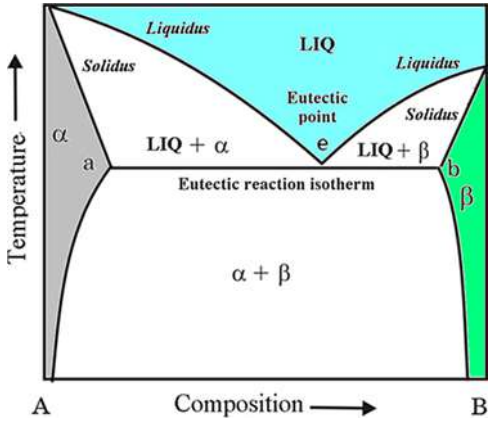

FIGURE 3.12 Eutectic equilibrium phase diagram with two solid solutions (A-rich α, B-rich ß). Maximal solubility of B in α-A is observed at eutectic temperature (point "a") and maximal solubility of A in ß-B is observed at point "b." Eutectic composition is marked by "e."

The peritectic systems have a transformation that occurs during heating as decomposition turns one of the solid phases into a liquid and a new solid phase—that is, the solid phase melts incongruently (with decay; see Fig. 3.10). In the peritectoid reaction, a similar process includes decomposition of the solid phase into two new solid phases upon heating.

For a system with more than two components, three-dimensional representation is normally needed. The composition coordinates are located in the horizontal plane (a triangle for a ternary system) and temperature is the vertical coordinate. Figure 3.14 shows a schematic of the FeO-MnO-SiO_2 system used to describe slags of ferromanganese and ferro-silicon-manganese processing. Here, different zones of the compounds can be seen together with a silica-rich, two-liquids immiscibility region (dashed lines).

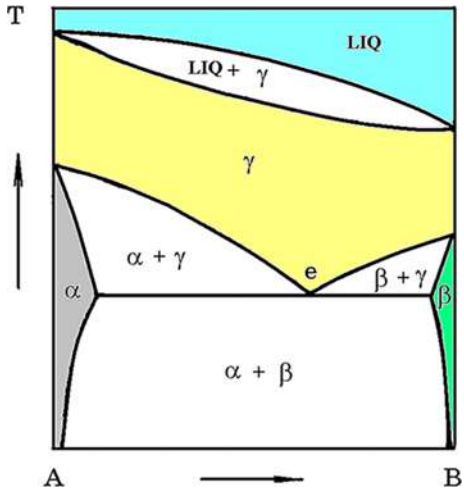

FIGURE 3.13 Eutectoid equilibrium phase diagram with three solid solutions (α, ß, γ). The eutectoid point is marked by "e."

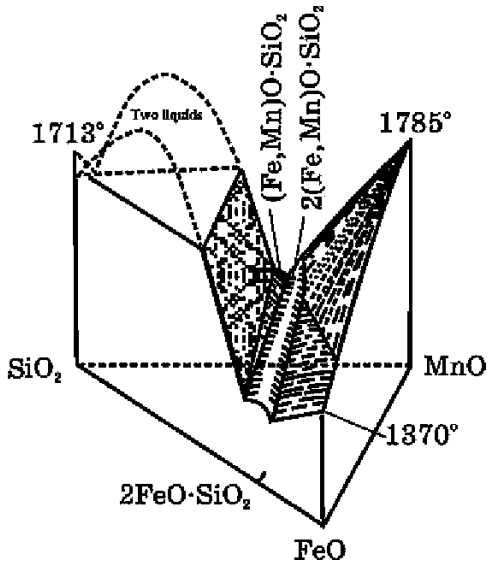

FIGURE 3.14 The schematics of the ternary FeO-MnO-SiO_2 system. *(From Gasik et al., 2009.)*

Systems with four or more components are difficult to represent in three-dimensional space and usually minor components' compositions are fixed, allowing variation of only compounds of interest.

3.1.4 Kinetics of Pyrometallurgical Processes

The reaction environment for ferroalloys production is complex. At low temperatures, where alloy containing oxide phases are solid, the direct solid-

solid reaction between carbon and oxides is very slow (the reactions with other reductants [Si, Al] proceed under different conditions, mentioned later). The reduction is carried out mostly by CO and H_2 (if there is moisture in the charge). In that case the reduction is a combination of oxide reduction by CO and its regeneration by the reaction of CO_2 with carbon (Fig. 3.15).

At higher temperatures when liquid phases are formed, the reduction is carried out by solid carbon in the carbon/slag interfaces and by carbon monoxide bubbling through the slag (including CO formed by carbon from electrodes). The reaction rate in that case is very complex and depends on many factors such as fluid flow and mixing intensity in slag; slag viscosity; the size of and distribution of carbon particles in the slag; and the amount, size, and distribution of CO and CO_2 bubbles in slag. So it is difficult to analyze and quantitatively describe the kinetics of reduction smelting in ferroalloys production.

There are a variety of reaction mechanisms, often based on different methods of heat and mass transfer. Reaction mechanisms may consist of the diffusion of one reactant through a product layer, external mass transfer (via diffusion, migration, convection, etc.) in the environment, thermal diffusion (heat transfer), adsorption, absorption, and desorption stages. These mechanisms may change if the reactant's state or condition changes. Most reactions in metallurgy are between solids and fluids in which the solid participates as a reactant that undergoes chemical changes. The overall fluid–solid reaction involves a combination of the following individual steps (Flammersheim and Opfermann, 1999):

- Transfer of the fluid reactants and the fluid products between the bulk fluid and the external surface of the solid particle
- Diffusion of the fluid reactants and the fluid products within the pores of the solid, if the solid contains open porosity

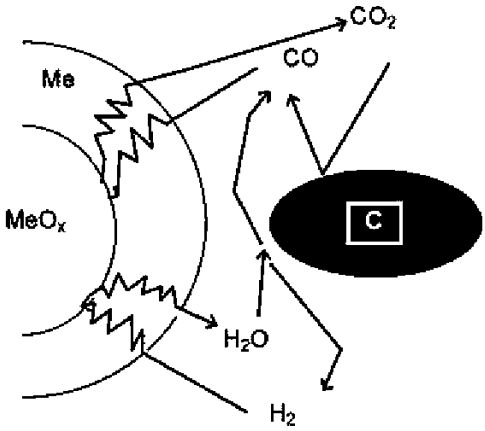

FIGURE 3.15 The schematic of the solid-state reduction of a metal oxide with CO and hydrogen in the presence of solid carbon. *(From Gasik, 2001.)*

- Chemical reaction between the fluid reactant and the solid at the fluid–solid interface
- Transfer of the reaction heat within the solid
- Transfer of heat between the external surface of the solid and the surroundings by convection and radiation
- Changes in the structure of the solid resulting from chemical reaction and heat.

These stages might be roughly allocated to the generic scheme shown in Figure 3.15, and it is understood that every such stage may have its own kinetics. Nevertheless, it might be possible to apply some principles of formal chemical kinetics to describe the overall reaction rate, even if it cannot possibly show the right reaction mechanism. In some cases, this formal reaction rate gives a hint about the limiting stage of the process (e.g., whether the overall reaction rate is limited by diffusion, surface of the reaction interface, or the transformation kinetics) and therefore possibilities for its improvement.

Reduction of iron-based and nonferrous oxide raw materials plays an important role in chemical metallurgy, because they relate to the production of metals from natural and secondary materials. Most raw materials are used in the form of oxide concentrates (iron ore, manganese ore, chromite, etc.) or pure (enriched) oxides (W, Mo, etc.). Kinetic peculiarities of reduction are also of great interest, and they are the bases for the development of industrially feasible technology and equipment. On the lab scale, kinetics is often studied by thermal analysis, which has been used in many areas of metallurgy to great advantage for explaining metallurgical processes. Its applications are in a range of studies of ores, oxides, scales, semifinished products, ferroalloys, and steels, as well as in studies on the reduction and oxidation of metals.

The application of kinetic analysis to reduction reactions includes two basic aspects. Scientifically, it includes the establishment of individual steps of the entire process as a model, as well as their clarification and interpretation. Technically the kinetic analysis is important as a tool for data extraction from measurements to provide an adequate kinetic model with minimum parameters. This kinetic model could be further applied for the process of prediction and optimization. In formal chemical kinetics, "reaction rate" usually means the rate of formation/destruction of the reagents in a certain period of time. For example, for a reversible reaction of the wüstite reduction by CO, as shown earlier for the thermodynamics of ferronickel formation (20): 'FeO' + CO ↔ Fe + CO_2 , the reaction rate is

$$v_P = \left\{-\frac{dN_{FeO}}{d\tau}\right\}_d - \left\{\frac{dN_{FeO}}{d\tau}\right\}_r = \left\{-\frac{dN_{CO}}{d\tau}\right\}_d - \left\{\frac{dN_{CO}}{d\tau}\right\}_r = \left\{\frac{dN_{Fe}}{d\tau}\right\}_d - \left\{-\frac{dN_{Fe}}{d\tau}\right\}_r = \left\{\frac{dN_{CO_2}}{d\tau}\right\}_d - \left\{-\frac{dN_{CO_2}}{d\tau}\right\}_r,$$

where N_i is the instant amount of moles of the component i, τ is the time, and v_P is the reduction rate. Subscript d refers to the direct reaction and r refers to the

reverse reaction. In the equilibrium, the rates of direct reaction (reduction of iron oxide) and the reverse reaction (oxidation of iron) are equal, and the resulting Gibbs energy change (20) is zero. Experimentally it was observed that for reactions the rate depends on the concentration of the starting compounds and temperature (if all other parameters are equal):

$$v_P = k_d \left[n_{FeO}\right]^{a1} \left[n_{CO}\right]^{b1} - k_r \left[n_{FeO}\right]^{a2} \left[n_{CO}\right]^{b2} , \tag{23}$$

where k_d and k_r are direct and reverse reaction rate constants, n_i is the concentration of component i, and $a1 \ldots b2$ refer to the reaction rate exponents. It is important to note that these exponents usually are in no way related to the stoichiometry coefficients of the reaction. To get the reduction rate, the differential equation (23) should be solved as a function of time, temperature, and components' concentration. However, simplified equations like (23) are very rare in real kinetic process analysis. To extend the formal mechanism for other reduction reaction types, let's start with a reaction equation in a general form:

$$v_1 A + v_2 B = v_3 D + v_4 E; \quad \frac{\partial [A]}{\partial \tau} = -\Phi(\tau, T, [A], [B], [D], [E]), \tag{24}$$

where $[X]$ refers to concentrations of components (A and B are the starting compounds; D and E are the reaction products), τ refers to time, T is the temperature, and Φ is a conversion function (Flammersheim and Opfermann, 1999). With certain limitations, it is possible to apply the Arrhenius theory for (24), although this procedure is not rigorously justified. It is further assumed that the conversion function can be described by two separable functions, k for Arrhenius-type dependence and f for mechanism dependence: $\Phi(\tau, T(\tau), [A],[B],[D],[E]) = k(T(\tau)) \cdot f([A],[B])$. The complete separation of variables in this differential equation is only possible for one-step processes. For the reaction rate function $k(T(\tau))$, several types of the equation have been suggested in the form of

$$k(T(\tau)) = A_r \cdot (T(\tau))^m \exp\left(-\frac{E_r}{RT(\tau)}\right), \tag{25}$$

where A_r is the frequency factor, 1/s, E_r is the activation energy (J/mol), R is the the universal gas constant (8.314 J/mol·K), and T is the time-dependent temperature. The exponent m in (25) depends on the consideration of the mechanism of reaction: the collision theory predicts $m = {}^1/_2$, in the theory of the activated state $m = 1$, and in the classical Arrhenius theory $m = 0$. Table 3.6 lists a series of the most typical reaction types along with their f functions. This list contains classic homogeneous reactions and typical solid-state reactions and their definitions (Brown et al., 1980; Flammersheim and Opfermann, 1999). The parameter α here means normalized reaction extent (it is zero if no reaction has yet taken place and unity when the reaction has completed).

Practical analysis of the kinetics of reduction or transformation is commonly made using thermal analysis (TA) methods. These methods and their use are defined in several DIN, CEN, and ASTM standards. Thermal

TABLE 3.6 Reaction Types and Equations for Reaction Rate $\partial\alpha/\partial\tau = -A_r\exp(-E_r/(RT))\cdot f(\alpha, 1-\alpha)$

$f(\alpha, 1-\alpha)$	Reaction Type
α	First-order reaction
α^2	Second-order reaction
α^n	n^{th} order reaction
$2\cdot\alpha^{1/2}$	2-D phase boundary reaction
$3\cdot\alpha^{2/3}$	3-D phase boundary reaction
$1/(2(1-\alpha))$	1-D diffusion
$-1/\ln(\alpha)$	2-D diffusion
$3\cdot\alpha^{1/3}(\alpha^{-1/3}-1)/2$	3-D diffusion (Jander's type)
$3/(\alpha^{-1/3}-1)/2$	3-D diffusion (the Ginstling-Brounstein type)
$2\cdot\alpha\cdot(-\ln(\alpha))^{1/2}$	2-D nucleation
$3\cdot\alpha\cdot(-\ln(\alpha))^{2/3}$	3-D nucleation
$n\cdot\alpha\cdot(-\ln(\alpha))^{(n-1)/n}$	*n*-D nucleation/nucleus growth (Avrami/Erofeev)
$\alpha\cdot(1+K_{cat}\cdot(1-\alpha))$	First-order reaction with autocatalysis through the reactants

analysis is commonly defined as a group of techniques in which a physical property of a substance is measured as a function of temperature, while the substance is subjected to a controlled temperature program (Brown, 1989). The most used methods are thermogravimetry (TG; monitoring mass changes of the specimen), differential thermal analysis (DTA; monitoring temperature changes of the specimen versus reference), and differential scanning calorimetry (DSC; monitoring the heat flux needed to keep the temperature of the specimen closest to the temperature of the reference). Several methods could be combined into a single measuring device; this is called "simultaneous thermal analysis" (STA). This combination also involves other techniques such as mass spectrometry (MS) or Fourier transform infrared spectrometry (FTIR).

Figure 3.16 shows an example of the kinetic data of the reduction of molybdenum trioxide at four different temperatures in the laboratory thermal balance, where mass change has been recorded in time. It shows that temperature from 700° to 800°C is not enough to reach complete reduction (relative mass change does not approach zero, as would be expected for the reaction $MoO_3 \rightarrow Mo$), staying at ~1/3 of the theoretical mass loss. This indicates that only 1 of 3 atoms of oxygen is removed and the final reduction product is MoO_2. At 900 to 1000°C, almost full reduction takes place, leading to metallic molybdenum.

This example is one of the simplest as there are no solid solutions, liquid phases, carbides, or other compounds formed. Realistic processes such as

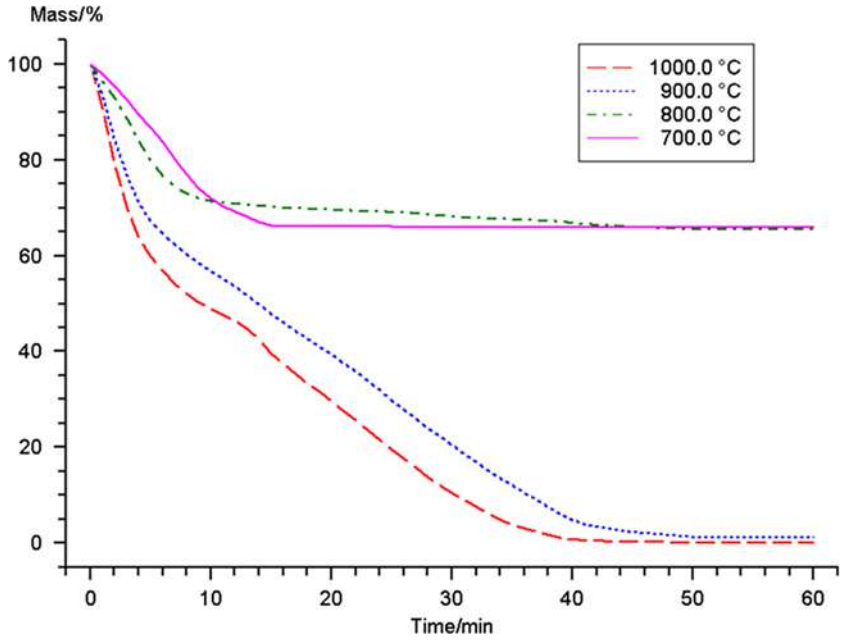

FIGURE 3.16 Kinetics of the reduction of molybdenum trioxide (relative mass, %) at four different temperatures in the laboratory thermal balance. *(Uses data presented by Ostrik and Gasik, 1993.)*

reduction of chromites or manganese ore by carbon in the presence of iron and slag-forming phases are much more complex, and the identification of the thermal analysis data is far from trivial. Nevertheless such experimental information helps to point out possible process stages and potential side reactions such as evaporation of the material or formation of intermediates. To demonstrate, Figure 3.17 shows data on simultaneous thermal analysis of nickel laterite ore. Here, changes in mass of the specimen (TG, %), thermal effects (exothermic and endothermic, DSC), and the evolution of gases (integral Gram-Schmidt signal) are overlaid.

The figure shows that the mass loss curve has several stages and that some thermal effects are correlated with the release of gases (e.g., the endothermic effect around 100°C accompanied with peak of the gas absorption signal. This is possibly associated with the release of water vapor). The gases coming out of the specimen are identified via Fourier transform infrared (FTIR) spectrometry analysis (Fig. 3.18).

In Figure 3.19, the data from Figure 3.18 are projected onto a spectral map. It shows that a major water release takes place after about 1000 s upon heating (~90° to 120°C), coinciding with a significant mass loss (Fig. 3.17). A major CO_2 peak release—at around 2000 to 3000 s (~400° to 550°C)—is possibly associated with decomposition of carbonates in the ore sample. Using this type

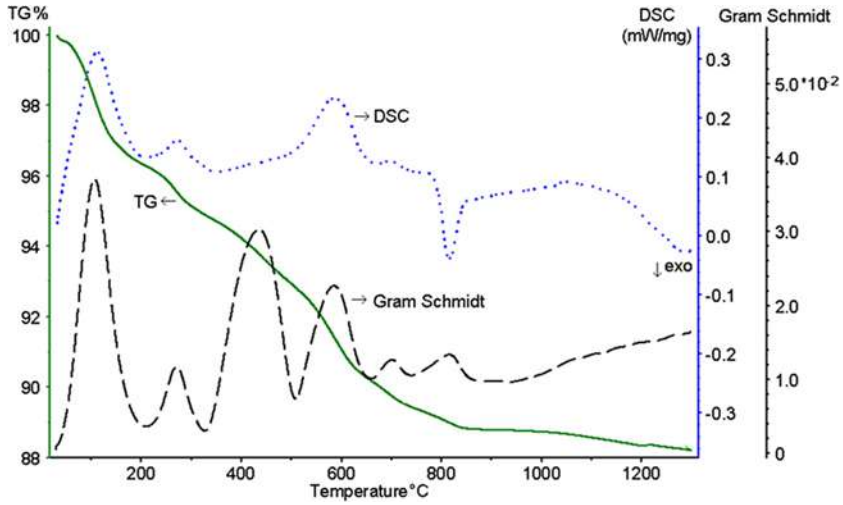

FIGURE 3.17 Kinetics of the transformation of nickel laterite ore at heating. Data are shown for mass loss (TG, %), thermal effects (DSC, mW/mg; exothermic reactions give a negative heat flux signal), and gases release (Gram-Schmidt trace, relative absorbance units; indicates degree of infrared absorption in the gas phase). *(Data provided by M. Gasik and M. Friman.)*

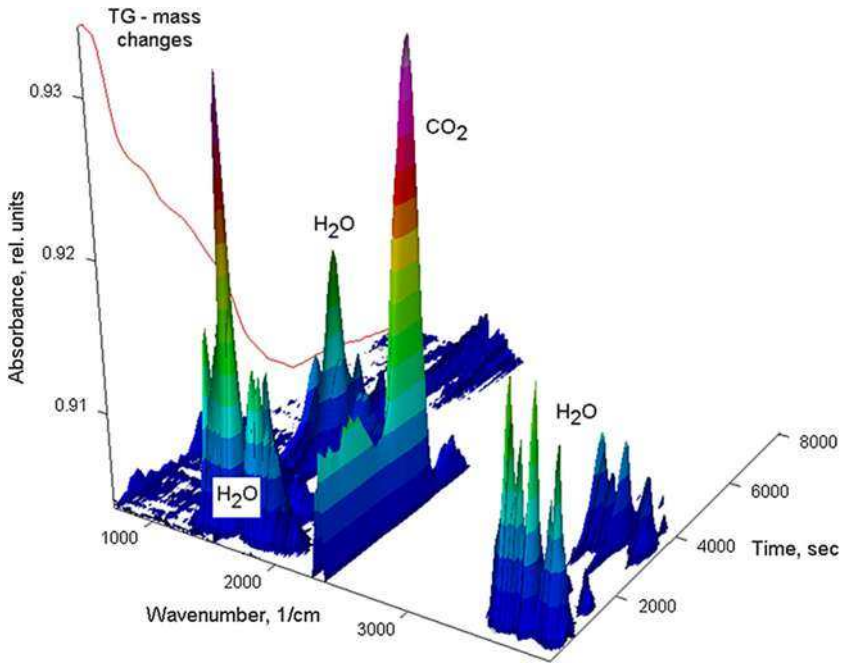

FIGURE 3.18 Example of gas evolution during the heating of nickel laterite ore (Fig. 3.17), where the spectral response of the Gram-Schmidt signal is expanded. Spectral areas of CO_2 and water are marked. The trace line on the left is the mass change (TG signal) from Figure 3.17.

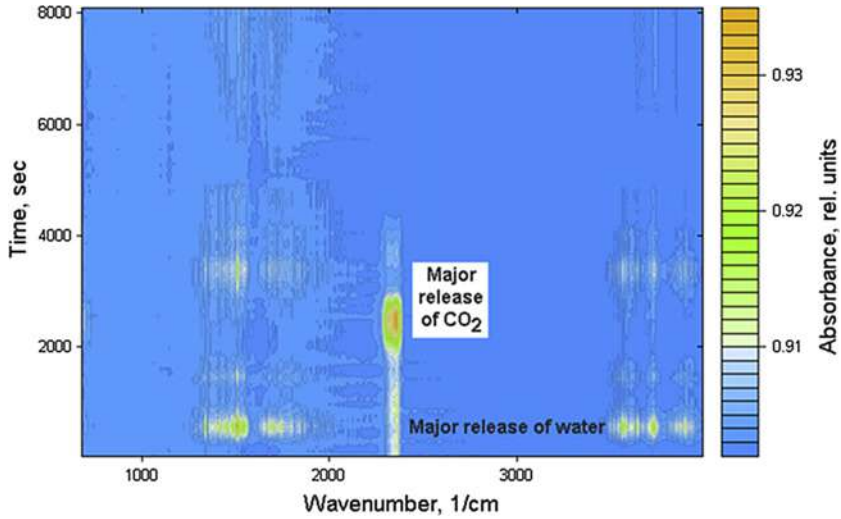

FIGURE 3.19 Projection of the process shown in Figure 3.18 indicating areas of major water and CO_2 release from laterite ore sample.

of thermal analysis, it might be possible to compare different specimens and to understand the processes behind the reduction of metal oxides and the production of ferroalloys.

3.1.5 Basics of Heat Transfer in Ferroalloys Processing

Heat and mass transfers are of extreme importance in all industrial processes, including ferroalloys smelting. Heat transfer includes the transportation of energy driven by temperature difference, and it might be realized by one of the following mechanisms (see Table 3.3): conduction, convection, and radiation. The first and third mechanisms do not involve mass transfer.

3.1.5.1 Heat Transfer via Conduction

Heat conduction in solids usually takes place via lattice vibrations (phonons) and electrons (especially in metals and semiconductors). Typical for heat conduction, the heat flux is proportional to the temperature gradient and material thermal conductivity (Fourier's law):

$$q\ \left[W/m^2\right] = -\lambda \nabla T. \tag{26}$$

For many solid materials, thermal conductivity might be approximated by a linear function of temperature—for example, for magnesite (MgO) brick in air, $\lambda = 6.16 - 0.00267 \cdot (T - 273)$ in W/(m·K). Let's suppose a smelting furnace has a cylindrical, multilayer wall (e.g., furnace steel shell, refractory lining, frozen charge or slag). In the stationary case (steady heat flux) across the wall, expanding equation (26), the resulting heat flow (in W/m^2) might be calculated as

$$q_{wall} = \frac{T_{in} - T_{out}}{\frac{1}{\alpha_{in} d_1} + \sum_{i=1}^{n-1} \frac{1}{2\lambda_i} \ln \frac{d_{i+1}}{d_i} + \frac{1}{\alpha_{out} d_n}}, \tag{27}$$

where d_i refers to the diameters of respective layers i, λ_i is the thermal conductivity of the i layer, and α_i is the convection coefficient inside and outside of the wall of the furnace. Convection coefficients are temperature dependent; for example, for a metallic shell or brick wall contacting with ambient air (20°C), $\alpha_{out} \sim 7.7743 + 0.0661 \cdot (T - 273)$, W/(m^{2}K), and this approximation already accounts for radiative losses as well. In high-temperature heat transfers, the inner convection coefficient is normally very high for turbulent flow and thus the term $1/\alpha_{in}$ might often be neglected.

3.1.5.2 Heat Transfer by Radiation

Heat transfer by radiation takes place through the transport of photons (electromagnetic radiation), which solid surfaces can absorb or reflect. Any body with a temperature above absolute zero emits thermal radiation. Surface-to-surface radiation may be hindered by shadowing and diffuse reflections between radiating surfaces. This is the only heat transfer mechanism able to operate in a vacuum and it requires only that photon flux reaches the surface. The radiative heat flux is proportional to material emissivity (degree of "gray") and the difference of absolute temperatures of emitter T_1 and receiver T_2 in fourth power (Stefan-Boltzmann law; $T_1 > T_2$):

$$q\left[W/m^2\right] = C_F \sigma \, \varepsilon_s \left(T_1^4 - T_2^4\right), \tag{28}$$

where $\sigma = 5.67 \cdot 10^{-8}$ W/(m^{2}K^4) is the Stefan-Boltzmann constant, C_F is the viewing (shading) coefficient (depending on a mutual arrangement of radiating and receiving surfaces), and ε_s is the total emissivity (unitless, 0–1). When the emissivity is unity, the heat flux emitted corresponds to the black body radiation. If radiative surfaces are somewhat obstructed or shadowed from the view of each other, the coefficient C_F is introduced, which accounts for this result so the effective heat flux is decreased. Some typical emissivities for different materials used in ferroalloys smelting are shown in Table 3.7.

3.1.5.3 Heat Transfer by Convection

Heat transfer via convection is now described for two scenarios. In the first, the fluid in motion carries away into some thermal energy, proportional to the net displacement of a fluid resulting from the fluid's own velocity (see Table 3.2):

$$q[W/m^2] = \int_{T_2}^{T_1} \mathbf{u} \cdot \rho \cdot C_P \, dT \approx \mathbf{u} \cdot \rho \cdot (C_P(T_1) \; T_1 - C_P(T_2) \; T_2), \tag{29}$$

TABLE 3.7 Typical Gray Body Emissivities for Some Materials

Material	Gray Emissivity	Temperature Range, °C
Aluminum, oxidized	0.11–0.19	200–600
Aluminum oxide (corundum)	0.23–0.4	1200–1700
Calcium oxide	0.27	800–1300
Carbon	0.79–0.81	100–650
Chromium oxide	0.73–0.97	800–1300
Copper, oxidized	0.57–0.87	200–600
Molybdenum	0.096–0.292	700–2600
Steel, polished	0.55–0.61	900–1100
Steel, oxidized	0.8	200–600
Tungsten	0.053–0.307	300–2200
Water	0.95–0.963	0–100

where fluid local velocity vector is **u**, fluid density ρ, and specific heat C_P, with temperatures at outlet and inlet, respectively, being given (density and velocity might be assumed constant if they do not significantly vary with temperature).

Another form of convective heat transfer occurs for heat dissipation from a solid surface to a fluid, where the heat transfer coefficient and the temperature difference across a hypothetical film describe the flux:

$$q\ \left[W/m^2\right] = \alpha_{conv}\cdot(T_{surf} - T_{fluid}), \tag{30}$$

where α_{conv} is the effective convection coefficient, and W/(m^{2}K) is defined in the same way as in (27).

3.1.5.4 Generalized Heat Transfer Equation

For a fluid, the resulting combined heat equation becomes

$$\rho C_P\left(\frac{\partial T}{\partial t} + (\mathbf{u}\cdot\nabla)T\right) = -(\nabla\cdot\mathbf{q}) + \sum_i\sum_j \tau_{ij}\mathbf{S}_{ij} - \frac{T}{\rho}\frac{\partial\rho}{\partial T}\bigg|_p\left(\frac{\partial p}{\partial t} + (\mathbf{u}\cdot\nabla)p\right) + Q_s, \tag{31}$$

where ρ is the density (kg/m^3), C_P is the specific heat at constant pressure (J/(kg·K)), **u** is the velocity vector (m/s), **q** is the conductive heat flux vector (W/m^2), p is pressure (Pa), τ is the viscous stress tensor (Pa), **S** is the strain rate tensor (1/s) equal to $^1/_2$ ($\nabla\mathbf{u}+\nabla\mathbf{u}^T$), and Q_s represents other heat sources, such as electromagnetic or joule heating (W/m^3). The other sources might also include terms such as those that have arisen from species diffusion (as the sum of partial

molar enthalpies by respective molar flux of the species), but these play a role only when there are species fluxes with substantially different enthalpies.

The generalized equation assumes that the mass of the fluid is conserved. The left part of the equation describes the rate of change of the stored heat (energy) in the material in time plus the contribution arising from convective heat inflow. The right part summarizes the contribution of conduction, radiation, viscous heating effects, and adiabatic heating from pressure work and other sources. In metallurgical practice, viscous heating and adiabatic heating are in most cases negligible and could be omitted.

For convection transfer between solid (walls) and fluid media, four cases might be outlined. They are combinations of either natural (no external forces besides gravity) or forced (blowing, mixing, etc.) convective fluid motion along an external (open) wall (surface) or an internal wall (tubes, pipes, closed reactors). Fluid flow in all these cases might be either laminar or turbulent. These conditions specify the dependence of the convection coefficient α_{conv}, for which no general expression could be made (Themelis, 1995). The determination of convective parameters is sometimes very complex, and the traditional engineering method relies on the use of different nondimensional groups (similarity numbers) (Table 3.8).

For natural convection arising within the closed volumes (between walls of different temperatures), a heat flux equation for thermal conductivity might be used, if thermal conductivity is corrected by the Rayleigh factor $q_c \approx \lambda \frac{T_1 - T_2}{S} \cdot 0.18(Ra)^{0.25}$. For forced convection, functional dependencies

TABLE 3.8 Some Important Nondimensional Numbers

Number	Formula	Use
Nusselt	$Nu = \frac{\alpha\ L}{\lambda} = = f(Gr, Re, Pr)$	Calculation of α from Nu value at given dimension L (pipe diameter, wall length, etc.) and fluid conductivity λ; gives the ratio of total heat transfer to conductive heat transfer
Grashof	$Gr = \frac{\beta\ L^3 g\rho\,\Delta T}{\mu}$	Fluid volume thermal expansion coefficient ß, density ρ, dynamic viscosity μ at given gravity g and temperature difference → ratio of buoyancy to viscous forces
Reynolds	$Re = \frac{u\ L\rho}{\mu}$	Fluid flow with velocity u → ratio of inertia to viscous forces; laminar flow usually if Re < 2300, turbulent for Re >5000; not used for natural convection
Rayleigh	$Ra = Pr \cdot Gr$	Ratio of natural bulk heat transport to convective heat transport (near walls of characteristic length L)
Prandtl	$Pr = \frac{\mu\ C_P}{\lambda}$	Ratio of momentum diffusivity to thermal diffusivity; for diatomic gases $Pr = 0.72$, for triatomic gases it is 0.8

of Nu are more complex. For example, a gas flowing around a flat plate at laminar conditions ($Re < 2300$ in pipes) has Nusselt number $Nu = 0.67\ Re^{0.5} Pr^{0.333}$ and the same for liquid metal under turbulent conditions ($Re > 5000$ in pipes) $Nu = 0.59\ Re^{0.61}$. More details about the nondimensional numbers and their application for heat and mass transfer coefficients normally relevant to metallurgical furnaces can be found in many handbooks (Bird et al., 2005; Incropera and De Witt, 1996; McCabe and Smith, 1976; Themelis, 1995; VDI, 1993).

3.1.5.5 Heat Generation

The last term in equation (31) is important for setting up the amount of heat (heat flow or power) generation in the metallurgical reactor (furnace), which is required to initiate, support, and fulfill the specific reduction reactions and to melt the charge and reaction products. This is connected with the power supply to a specific furnace and determines the size of the plant and the conditions for electrical transformers. In a set of six furnaces of 63 MVA-rated power, each easily may consume half of the power generated by a nuclear reactor station. Therefore, it is important to understand the principles of energy conversion into heat inside the furnace.

The properties of materials (charge components, metal, and slag) are usually temperature dependent, so equations like (31) become nonlinear. The electric current density vector in the furnace is expressed with the Maxwell-Ampere law:

$$\mathbf{J} = \nabla \times \mathbf{H} = \sigma\,(\mathbf{E} + \mathbf{u} \times \mathbf{B}) + i\,\omega\,\mathbf{D} + \mathbf{J}_{ext} \tag{32}$$

where σ is the electrical conductivity, $\mathbf{H}$ is the magnetic field strength, $\mathbf{E}$ is the electric field strength (the gradient of electrical potential $\nabla\varphi$), $\mathbf{u}$ is the velocity vector of the media (defining magneto-hydrodynamic flow), $\mathbf{B}$ is the magnetic induction, $\mathbf{J}_{\text{ext}}$ is the external current density (if present), $\omega = 2\pi f$ is the frequency of electrical field (Hz), and $\mathbf{D}$ is the electric displacement ($\mathbf{D} = \varepsilon \cdot \varepsilon_0 \cdot \mathbf{E} + \mathbf{P}$). Here ε is a real part of dielectric permittivity, ε_0 is the dielectric constant of the vacuum, and $\mathbf{P}$ is the polarization vector (which might be neglected for conducting materials). If the medium (slag, metal, charge) is not moving ($\mathbf{u} = 0$) and the voltage applied is DC only ($f = 0$), equation (32) transforms into Ohm's law (Gasik et al., 2010). The general Maxwell equations with use of (32) will take the following form:

$$\begin{aligned} &-\nabla\cdot\left(\left(i\,\omega\,\sigma - \omega^2\varepsilon\,\varepsilon_0\right)\mathbf{A} - \sigma\,\mathbf{u}\times(\nabla\times\mathbf{A}) + (\sigma + i\,\omega\,\varepsilon\,\varepsilon_0)\,\nabla\varphi\right. \\ &\quad \left. -\,(\,\mathbf{J}_{ext} + i\,\omega\,\mathbf{P})\right) = 0 \\ &\left(i\,\omega\,\sigma - \omega^2\varepsilon\,\varepsilon_0\right)\mathbf{A} + \nabla\times\left((\mu\,\mu_0)^{-1}\nabla\times\mathbf{A} - \mathbf{M}\right) - \sigma\,\mathbf{u}\times(\nabla\times\mathbf{A}) \\ &\quad + (\sigma + i\,\omega\,\varepsilon\,\varepsilon_0)\,\nabla\varphi = \mathbf{J}_{ext} + i\,\omega\,\mathbf{P} \end{aligned} \tag{33}$$

where $\mathbf{A}$ is the vector magnetic potential, $\mathbf{M}$ is the vector of the material's magnetic saturation, μ is the relative magnetic permittivity, and μ_0 is the

magnetic permittivity of the vacuum. These equations describe the complete electromagnetic behavior of current, potential, and magnetic parameters in any materials or media. When an electromagnetic field is interacting with a material, the power dissipated in that material has active (ohmic) and reactive (inductance, capacitance) parts. In metallurgical practice, only ohmic (joule) losses lead to material heating, unless high-frequency (RF or microwave fields) are used. The total power dissipation in the material in the domain Ω is defined by partial derivatives of electric and magnetic energies:

$$-\int_{\Omega}\left(\mathbf{E}\cdot\frac{\partial \mathbf{D}}{\partial t}+\mathbf{H}\cdot\frac{\partial \mathbf{B}}{\partial t}\right)d\Omega = \int_{\Omega}\mathbf{J}\cdot\mathbf{E}\ d\Omega+\oint_{S}(E\times H)\cdot\mathbf{n}\ dS, \tag{34}$$

with $\mathbf{n}$ being the normal vector to the bounding surface S. The first part of the right-hand side is cycle-time-averaged joule heating (ohmic losses), and the second is reactive power (especially inductive losses). This joule heating is the major source of the heat in the ferroalloys' smelting furnace, and it gives the major positive contribution to the source term Q_s in equation (31). Other heat sources and sinks are mostly heat from reactions (oxidation of carbon, enthalpy of reduction reactions, melting, and solidification), balanced by heat losses through the walls, roof, exhaust gases, and tapped materials.

3.1.6 Basics of Mass and Momentum Transfer in Ferroalloys Processing

Mass transfer is a critical aspect of ferroalloys processing, as it controls the conversion of raw substances into other final products. In ferroalloys processing, mass transfer occurs mostly through chemical reactions (which cause significant concentration gradients, acting as driving forces), via phase separation and transformation. Most ferroalloys processes require external heat, which in turn affects both the reactions themselves and other physical processes connected with the system. Furthermore, most furnace operations require an optimized and steady production of product. This means that most mass balance applications require coupling to momentum and energy balances.

3.1.6.1 Diffusive Mass Transfer

The simple mass balance equation for any species might be written for a change of the species concentration c_i (mol/m^3) in time:

$$\frac{\partial c_i}{\partial t} = \nabla\cdot(D_i\nabla c_i)-\mathbf{u}\cdot\nabla c_i+R_i, \tag{35}$$

where D_i is the species diffusion coefficient, $\mathbf{u}$ is the fluid velocity, and R_i is the respective reaction rate, which produces these species (as shown in the previous section for kinetics of the processes). The left-hand side and the first term on the right-hand side of equation (35) constitute Fick's law of diffusion. The

diffusion coefficients D (describing pure Fick's diffusion) are independent of concentration. However, in concentrated solutions or melts, where relative concentrations are of the same order of magnitude, all species interact with each other and themselves (Wesselingh and Krishna, 2000). Their diffusion coefficients are therefore species and concentration dependent, and they can also depend on temperature and pressure. In this case for n-component system, the complete diffusion process is described by the Maxwell-Stefan equation, expressing concentrations in terms of weight fractions (w_j) and molar fractions x_j (Bird et al., 2005; Wesselingh and Krishna, 2000):

$$\frac{\partial}{\partial t}(\rho w_i) + \nabla\cdot\left(\rho w_i\left(\mathbf{u} - \sum_{j=1}^{n}\tilde{D}_{ij}\left(\nabla x_j + \left(x_j - w_j\right)\frac{\nabla p}{p}\right)\right) - D_i^T\frac{\nabla T}{T}\right) = R_i,$$

$$x_j = \frac{w_j}{M_j}M_\Sigma, \qquad \sum_{j=1}^{n} w_j = 1. \tag{36}$$

This equation includes also possible effects of pressure and temperature gradients, which might be significant in different parts of the furnace (e.g., near electrode working tips). The difficulty in direct use of this equation is application of the Maxwell-Stefan cross-diffusion coefficients, which are related to the Fick cross-diffusion coefficients D_{ij} in a complex way, requiring numerical calculations. For example, for a three-component system

$$\tilde{D}_{ij} = \frac{\dfrac{w_1(w_2+w_3)}{x_1 D_{13}} + \dfrac{w_2(w_1+w_3)}{x_2 D_{23}} - \dfrac{(w_3)^2}{x_3 D_{12}}}{\dfrac{x_1}{D_{12}D_{13}} + \dfrac{x_2}{D_{12}D_{23}} + \dfrac{x_3}{D_{13}D_{23}}}. \tag{37}$$

Another contribution to the species diffusion in ferroalloys processing might be important, especially in the case of DC furnaces or other situations where there are strong electric fields acting on fluids with charged species (metal and slag melts). This is the Nernst-Planck contribution of electromigration of charged species under the gradient of electric field ∇V, changing diffusion equation (35) to

$$\frac{\partial c_i}{\partial t} = \nabla\cdot(D_i\nabla c_i) - \mathbf{u}\cdot\nabla c_i + Z_i v_i F c_i \nabla V + R_i. \tag{38}$$

Here the additional term includes species charge Z, species ionic mobility v (s·mol/kg), and $F = 96480$ C/mol, the Faraday number. This equation is complemented by the electroneutrality condition and the conservation of electric current: $\sum_j Z_j c_j = 0$; $\nabla\cdot\mathbf{i} = F\sum_j Z_j R_j$.

3.1.6.2 Convective Mass and Momentum Transfer

The generalized Navier-Stokes formation for fluid flow (in the absence of chemical reactions or phase changes) combines conservation of mass

$$\frac{\partial \rho}{\partial t} + \nabla \cdot (\rho \cdot \mathbf{u}) = 0, \tag{39}$$

conservation of momentum

$$\rho\left(\frac{\partial \mathbf{u}}{\partial t} + (\mathbf{u} \cdot \nabla)\mathbf{u}\right) = \nabla \cdot [-p\,\mathbf{I} + \tau] + \mathbf{F}, \tag{40}$$

and conservation of energy (equation (31)). Here, $\mathbf{I}$ is the unity tensor and $\mathbf{F}$ is an external body force (e.g., gravity) acting on that fluid (Hauke and Hughes, 1994). When the fluid might be considered incompressible (constant density during the flow), the incompressible Navier-Stokes formulation will take the following form:

$$\rho\left(\frac{\partial \mathbf{u}}{\partial t} + (\mathbf{u} \cdot \nabla)\mathbf{u}\right) = \nabla \cdot \left[-p\,\mathbf{I} + \eta\left(\nabla \mathbf{u} + (\nabla \mathbf{u})^T\right)\right] + \mathbf{F}. \tag{41}$$

These Navier-Stokes equations (40, 41) describe the basic phenomena of mass and momentum transport. This is the practical case for all fluids under normal conditions and also for gases at low velocities, unless pressure is getting too high. Because fluids in ferroalloys processing (slags, metals) pass through zones with large temperature gradients, this causes significant convection forces because of buoyancy. Physically, fluids density changes with temperature and it formally contradicts with incompressible assumption. To provide a solution, the Boussinesq approximation was developed to treat such cases of buoyant flows without having to use a compressible formulation of the Navier-Stokes equations (Hauke and Hughes, 1994). It assumes that variations in density have no effect on the flow field except that they give rise to buoyant forces. The density in equation (41) is taken to be a reference value (ρ_0), except in the body force term, which is set to $\mathbf{F} = \mathbf{g}(\rho_0 + \Delta\rho(T))$. The extra density changing term here is the density difference due to its volumetric thermal expansion. This allows solution of differential equation (41) and determination of fluid velocities. The same formulation can be used for turbulent flow simulations, although in that case it requires the use of the averaged equations, resulting in a hierarchy of equations and statistical unknowns. To solve these equations for turbulent flow (high Reynolds number values), different models have been developed, such as the k-ε turbulence model (Hauke and Hughes, 1994). Solutions that involve Reynolds-averaged equations require dedicated computational fluid dynamics (CFD) algorithms.

3.2 FERROALLOYS COMPONENTS AND THEIR PROPERTIES

3.2.1 Metallic Melts

Metallic melts form in every ferroalloy process and they are the main product with targeted composition upon solidification. The structure of the metallic melt is a subject of intensive studies. According to common knowledge, the

structure of liquid metals and alloys consists of a short-range ordered packing of atoms, which is close to the same coordination structure as the same alloy in the solid nearly its melting temperature. This is usually analyzed by measuring the radial distribution function with various diffraction methods.

As many ferroalloy systems have several metallic elements in the solution, there is no simple or straightforward model that allows description of the atoms' location and their interaction with temperature and composition. A comprehensive review of the thermodynamic, quasi-chemical, and statistical models of metal melts is given, for instance, by Lupis (1983), Hillert (1998), Kubaschewski and Alcock (1979), and other publications. Experimental data clearly show that liquid alloys do have complex structures, which change with temperature and composition (Seetharaman and Sichen, 1994). This is reflected in the variation of all properties (viscosity, surface tension, electric conductivity, density, etc.). For example, the data for the liquid Fe-Si alloys show that for Fe-25% at. Si, the primary solid phase is α'-Fe_3Si but the liquid phase has a "mixture" of subsystems based on Fe and FeSi associates (Zubov and Gasik, 2002). For the melt of ε-FeSi phase, the liquid has ~90% of ε-FeSi associates and ~10% of chaotic (Fe,Si) liquid, whereas $FeSi_{2.3}$ phase has, in the liquid state, chaotic (disordered) liquid (Fe,Si), quasi-eutectic FeSi-Si, and "extra" silicon atoms. Knowledge of the liquid melts' structure and composition is very important for selecting the proper ferroalloy composition, not only from the view of processing (lower metal activity) but in terms of the stability of the alloy as well (it should not disintegrate or undergo oxidation after tapping and storage).

In some cases, minor impurities are also important to control from the point of view of safety of ferroalloys handling. One of the well-known cases is phosphorus and arsenic impurities in high-silicon FeSi, forming phosphides and arsenides, which react with moisture releasing highly toxic PH_3 and AsH_3. Therefore, special norms were elaborated regulating marine transportation of FeSi alloys in closed compartments (Zubov and Gasik, 2002) to avoid personnel poisoning.

Thus, the role of metal solutions formation during ferroalloys smelting is essential and might be summarized as follows:

- When the metal is dissolved into another melt (its activity decreases), the Gibbs energy change of the reduction and dissolution reaction is more favorable for recovery of the metal from its oxide. The maximal benefit is achieved when the melt composition approaches the similar one as for the most stable compound in the system.
- The total free energy decrease leads to lowering of the reduction temperature, which requires less energy input.
- Decrease of metal activity means its lower partial pressure, which decreases metal loss with gas phase and vapors.
- Melt with lower activity does not react with CO gas to the same extent as pure metal, which in many cases might lead to undesired secondary carbides formation (e.g., $2Al + CO \rightarrow Al_2OC$ or $7Cr + 6CO \rightarrow Cr_7C_3 + 3CO_2$).

- Introduction of dissolving metals allows formation of a ferroalloy of correct composition and properties, ensuring an optimal smelting process.
- Formation of the complex melt allows co-reduction of several elements and makes it possible to receive ferroalloys with several elements (FeSiCr, FeSiMn, FeSiAl, etc.), which are otherwise difficult or not economic to produce separately (for example, there has been a proposal to receive pure manganese and silicon separately and then mix them together to alloy or deoxidize steel).

3.2.2 Oxide Melts (Slags and Fluxes)

Ferroalloy slags usually contain SiO_2, ferroalloy metal oxides (MeO_x–process dependent, i.e., Mn, Cr, etc.), basic oxides (CaO, MgO, FeO, alkalis), and additional compounds (Al_2O_3, P_2O_5, S). Silica in slag melts is presented in tetrahedral units based on the $[SiO_4]^{4-}$ anion. There are five possible forms of silica tetrahedrons, the base tetrahedron $[SiO_4]^{4-}$ and four other types $[SiO_4]_n^{m-}$, where the number of joint apexes $n = 1\ldots4$ and charges $m = 4\text{-}n$ (Gasik et al., 2009). The molar ratio of SiO_2 to the sum of metal oxides indicates the degree of polymerization (oligomerization, or short chain formation). It might be expressed by the reaction $nSiO_4^{4-} \rightarrow Si_nO_{3n+1-c}^{2(n+1-c)} + (n-1+c)O^{2-}$, taking into account the isomerization of silicate structures and formation of the complex tetrahedron networks.

Each metal oxide is considered to break a bond of the network of tetrahedral units by supplying an additional oxygen and charge, compensating the electron at the broken bond with the cation (Sridhar, 2002). When the ratio is equal to two, each tetrahedral unit has one unshared corner, leading to the network structure resembling an endless sheet. When the ration decreases toward unity, the structure turns into endless chains (Sridhar, 2002). At lower ratios, the network breaks down further to form rings and ring groups and finally discrete units of silica compounds (Gasik et al., 2009), as shown in Table 3.9.

In complex silicates, alumina as amphoteric oxide accommodates itself in the silica network in silica-rich melts as AlO_4^{5-}, but it changes its role as network breaker in low-silica melts. Phosphorus oxide substitutes alkalis and integrates in the silica network as PO_4^{4-} (Sridhar, 2002). Besides the ratio of silica to metal oxides, metal cation charge and size also play a role: smaller size (Fe^{2+}, Mg^{2+}) and higher charge (Fe^{3+}, Al^{3+}) promote formation of (di)orthosilicates.

During ferroalloy smelting, the charge heats up and minerals start to react with each other. The lowest melting temperature compounds that are present or form in the charge establish the liquid phase, whereas other charge components remain solid. If the composition has many low-melting temperature phases (e.g., manganese ferroalloys with MnO-SiO_2 system), the first liquid slag phase forms in the top part of the charge in the furnace (for high carbon ferromanganese about 150 to 250 mm below the charge level). There, carbon starts to reduce oxides from the liquid slag. When the charge consists of components with high melting temperatures (in production of FeSi, SiCa, FeSiAl, or high

TABLE 3.9 Types of Silicate Network Structures Formed in the Slags (see Gasik et al., 2009)

Silicate	Example	Tetrahedron Type
Ortho	Olivine $(Fe,Mg)_2[SiO_4]$	Isolated
Di-ortho	Aksinite $Ca_2(Mg,Fe)Al_2[Si_2O_6]_2BO_3$	Twinned
Ring	$[Si_3O_9]^{6-}$, $[Si_4O_{12}]^{8-}$, $[Si_6O_{18}]^{12-}$, $[Si_{12}O_{20}]^{12-}$	Ring groups of 3, 4, 6, and 12 (6 + 6)
Chain	Wollastonite $CaSiO_3$, rhodonite $MnSiO_3$	Finite single-phase 1D chains
Ribbon I	Tremolite $Ca_2Mg_5[Si_4O_{11}]_3(OH)_2$	Ribbon formed by 1D chains
Ribbon II	Talc $Mg_3[Si_4O_{10}](OH)_2$	Ribbons formed by 1D layers
Skeleton	Nepheline $KNa_3Al_4Si_4O_{16}$	Bonds formed by oxygen atoms

carbon FeCr), the liquid slag phase forms well below the charge level. There, substantial gas cavities form under electrodes where electric arcs are operating. In some cases (smelting of high carbon FeMn and FeSiMn), the furnace operates in the arc-less mode when electrodes are immersed in the slag and the heating proceeds in the resistance mode (joule heating), although some micro-arcs appear there locally because of variations in temperature (Gasik et al., 2009). Among the set of properties of ferroalloy slags, two parameters are the most critical for the smelting process: slag viscosity and electric conductivity.

3.2.2.2 Viscous Properties of Slags

The flow behavior of slags is an important factor in many metallurgical systems, influencing the efficiency of separation of slag from metal and matte phases, the extent of slag foaming, and the kinetics of metal smelting and refining reactions (Kondratiev et al., 2002). Viscosity (η, Pa·s) is a measure of the ability of a fluid to sustain shear stresses, and in most cases viscosities are independent of the shear rate (Newtonian fluids, described by the incompressible Navier-Stokes equation (38)). The viscosity links the shear stress and the fluid velocity gradient normal to the shear stress vector (Shridhar, 2002). Shearing of layers of a fluid involves bonds breaking, and thus viscosity is a thermally activated process, often expressed as an Arrhenius-type relationship characterized by a preexponential factor A and an activation energy E:

$$\ln \eta = \ln A + \frac{E}{RT} \tag{42}$$

The ranges of viscosities that are typically encountered in metallurgical systems include 10^{-3}–10^{-2} Pa·s for liquid metals and 10^{-2} to 10^{10} Pa·s for slags. If the slag needs to be tapped from the furnace, its viscosity should be lower than 15 to 25 Pa·s for the free flow. Experimental methods of viscosity and other determinations of the thermophysical properties of slags have been reviewed by Aune et al. (2002) and for metallic melts by Seetharaman and Sichen (1994). A summary covering most of the published viscosity models suitable for use in metallurgical applications is given by Kondratiev et al. (2002) and Sridhar (2002).

Many models have been developed for predicting viscosity from chemical compositions and temperature; however, the performance of the various models varies depending on the range of viscosity covered. The current understanding of the structure of slags is insufficient to construct a reliable model, one capable of encompassing a wider range in viscosity (Sridhar, 2002). For engineering purposes, a correlation was suggested by Gasik and Gasik (2010)—first for electrical conductivity and later also for viscosity; it was recognized that the preexponential factor A in Arrhenius equation (39) is not constant but that it follows the Meyer-Neldel rule (Meyer and Neldel, 1937). This rule posits a linear dependence of the logarithm of A versus activation energy, so equation (42) might be rewritten as

$$\ln \eta = a_0 - \frac{E}{RT_0} + \frac{E}{RT}, \tag{43}$$

where a_0 is the true constant and T_0 is the characteristic Meyer-Neldel temperature (isokinetic temperature), when the parameter (viscosity in this case) is not dependent on the activation energy. The physics behind this rule is not clear, although different explanations have been suggested (Dyre, 1986). This dependence is known to be very fundamental and has been observed in different materials and conditions, including the diffusion process (Swalin, 1956). Gasik and Gasik (2010) analyzed data for different slags (Fig. 3.20) and found that almost all ferroalloy slag viscosities might be approximated using the equation

$$\eta = 0.1771 \exp\left(\frac{E}{R}\left(\frac{1}{T} - \frac{1}{2008}\right)\right), \tag{44}$$

where activation energy is composition-dependent. It was thought that this behavior might be due to formation of the silicate networks in slags, but it also holds in fluxes, which have no silica.

Using advanced statistical methods, it is possible to arrive at a prediction of the activation energy versus slag composition (Fig. 3.21), although more experimental data are needed to improve the reliability of this analysis (Gasik and Gasik, 2010).

3.2.2.3 Electrical Conductivity of Slags

Electrical conductivity of molten slags is critical for the correct selection of ferroalloys for the operation of furnaces. There are different theoretical models of

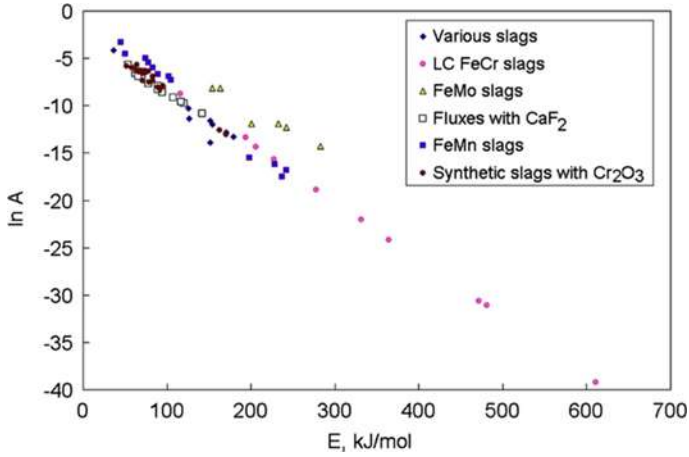

FIGURE 3.20 Dependence of the preexponential factor (ln A) on activation energy E for the viscous flow of different ferroalloy slags. *(Data collected by M. Gasik.)*

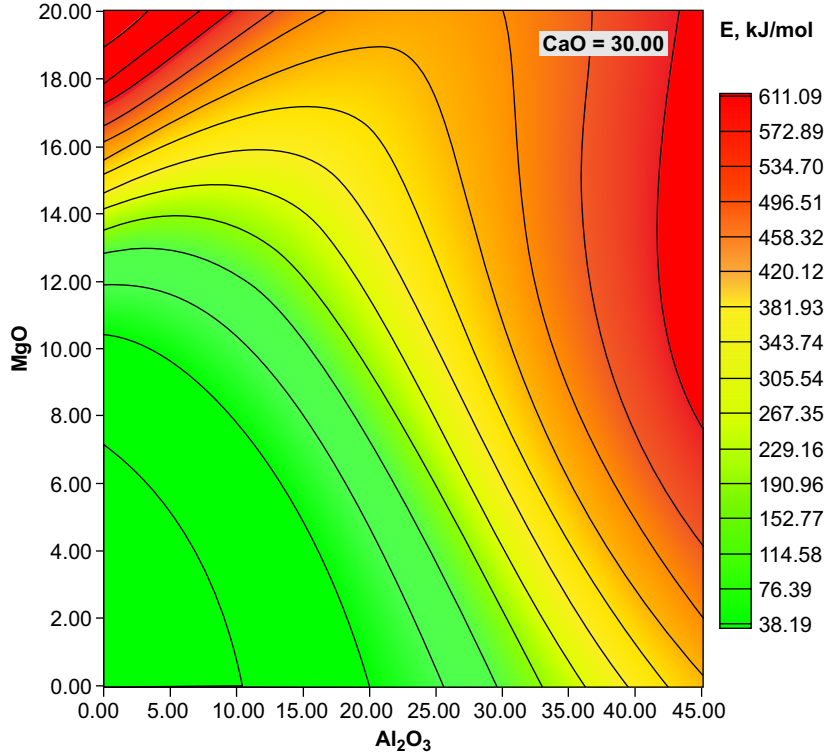

FIGURE 3.21 Predicted activation energy for the viscous flow of the MgO-Al_2O_3-30%CaO slags. Note this is just an illustrative example and should not be used in calculations. *(Data provided by M. Gasik.)*

the electrical conductivity of slags, based either on their treatments as ionic liquids (electrolytes) or on more simplified phenomenological correlations such as approximation using Stokes-Einstein-Nernst equations. However, in complex ionic melts it is difficult to assign specific values to parameters such as "particle radius" or "number of particles per unit volume with specific charge." Many silicate slags exhibit complicated oligomerization of silicate networks where the "particle" definition makes little sense. The concept of optical basicity was intensively applied earlier, but as stated, it is not scientifically justified for slags with transition metals, which are essentially the basis of ferroalloys production.

For example, Segers et al. (1978) have experimentally measured electrical conductivities of the liquid slags in the CaO-MnO-SiO_2 system and represented specific electrical conductivity χ recalculated into equivalent conductivity Λ:

$$\Lambda = \frac{\chi V_m}{2(1 - N_{SiO_2})},\ \ln \chi = \ln A + \frac{E}{RT}, \tag{45}$$

where V_m is the liquid slag molar volume, m^3/mol, and N_{SiO_2} is the molar fraction of SiO_2. Equation (45) assumes that the electrical conductivity of slags using this system is ruled mostly by Ca^{2+} and Mn^{2+} (hence, in equation (45) the divider is 2 because of valence number 2+). Silica was assumed to exist in more complex tetrahedron forms like SiO_4^{4-} or $Si_2O_7^{6-}$, and its effect on electrical transport was neglected. The data obtained by Segers et al. (1978) exhibited significant nonlinearity versus SiO_2 concentration or versus the "manganese module" $t = N_{MnO}/(N_{MnO}+N_{CaO}) = N_{MnO}/(1 - N_{SiO_2})$. Later analysis of these data (Gasik and Gavrilov, 2001) did not reveal such correlations of these plots with thermodynamic properties of these slags; neither did it show a clear dependence of the composition. Also questioned was the extent to which the assumption of basic +2 charge carriers is valid only within the whole composition range and the temperatures studied. The charge transfer in electrolytes must obey electroneutrality, even if partial charge transfer numbers might be different for different cations and anions.

By using an approach similar to the treatment of viscosity described earlier, Gasik and Gasik (2010) have shown that the electric conductivity of liquid slags also follows the Meyer-Neldel rule (Dyre, 1986; Meyer and Neldel, 1937). Figure 3.22 shows the dependence of the preexponential factor on the activation energy of electrical conductivity.

For the system CaO-MnO-SiO_2, electrical conductivity (Sm/cm) might be expressed as

$$\chi \approx 23.6\ \exp\left(-\frac{E}{R}\ \left(\frac{1}{T} - \frac{1}{3550}\right)\right), \tag{46}$$

where activation energy depends on slag composition and might be predicted using advanced statistical analysis, for which rather good correlations have been obtained (Gasik and Gasik, 2010).

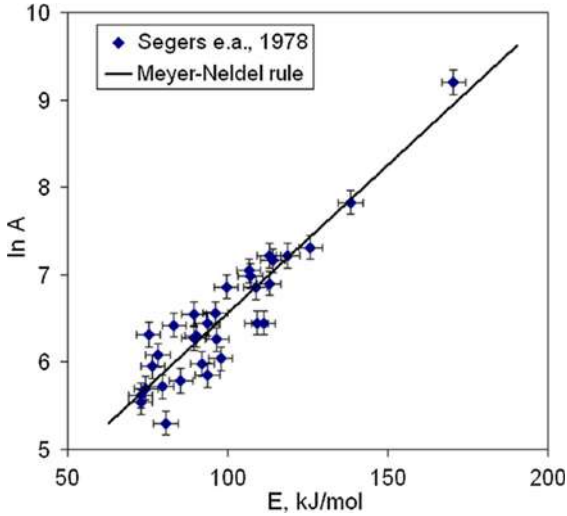

FIGURE 3.22 Dependence of the preexponential factor (ln *A*) on activation energy *E* for the electric conductivity of slags of form CaO-MnO-SiO_2. *(Based on the work of Gasik and Gasik, 2010.)*

3.2.3 Carbon Reductants for Ferroalloys Processing

Carbon reductants play a critical role in ferroalloys processing. The basic requirements for the quality of carbon reductants are different for various ferroalloy groups and include the following indicators: (1) composition (solid [nonvolatile] carbon, volatile matter, moisture, and sulfur), (2) the amount and chemical composition of the ash (nonreducible oxides), (3) electrical resistance, (4) porosity, (5) physical and mechanical properties (size distribution, strength characteristics), and (6) reduction ability in respect to the oxides of the element in question.

According to the modern classification of raw carbons, there are several phases, which have different microstructure, properties, and possibly different geneses. Table 3.10 presents one of the known classifications based on different carbon mineral constituents, which are commonly found in coals (Zubov et al., 2001). Vitrinite components are usually the most important for determining the quality of produced metallurgical coke.

In Table 3.11 are listed some commonly used carbon reductant properties. However, these properties might vary for different producers depending on the carbon source, so this table gives a rather general idea about the differences in the reductant properties.

The reducing ability of carbon reductant is one of the most critical parameters, in addition to its electric resistance. The feasibility of a particular reducing agent to produce a specific type of ferroalloy is determined during industrial tests. Carbon reductant should have less potential for graphitization, because it causes a decrease in the reactivity of carbon, electrical resistance, and surface area, all of which affect the ability of the carbonaceous material to recover metals from oxides.

TABLE 3.10 Classification of Different Coal Components

Group	Characteristics
Vitrinite (V), semi-vitrinite (SV)	Glossy, colloidal structure; glassy fracture surface
Fusain or fusinite (F)	Tissue-like fiber and sooty structures
Liptinite (L)	Matt structures where soluble components were eluted
Alginite (ALG)	Products from organic-walled marine microfossils
Mineral impurities	Clay minerals, iron sulfides, carbonates, and the like

TABLE 3.11 Comparison of Properties of Different Carbon Reductants

Parameter	Coke	Nut-Coke	Half-Coke	Petrocoke	Charcoal
Ash A^d (% wt.)	8–11	8–11	22–27	<1	<2
Volatiles VOC (% wt.)	<2	<1.5	4–6	7-9	10–15
Moisture W^p (% wt.)	<0.5	<1.5	<2	<1	1.5–2.5
Total sulfur S, (% wt.)	<1	<1.5	<1	1–5	<0.05
Solid carbon C_t	>85	>85	>70	>85	>80
Reactivity at 1323 K, ml/(g·s)	>0.5	>0.9	>8	>0.3	>10
Resistivity, Ohm·m, for 3–6 mm	1–2	1–2	7500	$3 \cdot 10^6$	$2 \cdot 10^6$
Structural strength, %	>80	>85	>62	>62	>35
Density, g/cm^3, real/apparent	1.82/0.91	1.95/0.93	1.58/0.93	1.41/1.12	1.4/0.40
Porosity, %/cm^3/g	53.1/0.49	49.7/0.51	55.0/0.67	20.1/0.18	63.8/1.1
Ash composition, % wt.:					
SiO_2	33–37	35–37	75–78	45–48	<2
Al_2O_3	20–25	21–23	10–12	23–26	<4
$CaO + MgO$	3–5	3–5	3–5	9–11	40–45
Fe_2O_3	30–35	30–35	7–9	13–15	<1
P_2O_5	0.1–0.3	0.1–0.3	<0.05	0.5–1.0	5–6
$K_2O + Na_2O$	2–2.5	2–2.5	1–2	0.1–0.2	<0.5

Electrical resistivity of a reductant also impacts the resistivity of the whole charge in the furnace. It depends on the number and size distribution of cokes (or other reductants), ores, concentrates, fluxes, additives, and other components of the charge. Reducing the size of pieces of coke and ore components

increases the resistivity. Excessive shrinkage reduces the permeability of the pieces of the charge, resulting in a drop in performance and the economic indicators of the ferroalloy smelting. In practice, optimal particle size distribution of the charge is determined as a result of testing in batch furnaces at different particle distributions. Technologically, the electrical resistance of the charge has to be kept high enough to reduce the amount of electric current passing through the charge in favor of the current passing through the electric arcs, as they are the main heat source in the furnace.

Contrary to requirements for low electrical conductivity of carbon materials as reductants, for manufacturing carbon-based electrodes (self-baked, graphitized, composite), specific electric resistance must be as low as possible (Brandtzæg, 1985). This is usually achieved by performing calcination (high-temperature treatment over 2000°C) of carbon raw materials such as anthracite. The transformation of amorphous structures of anthracite into crystalline (graphite-like) material at high temperatures reduces the electric resistance, density, specific heat, degree of graphitization (crystal size), ash, and the contents of volatile organic compounds (VOC) (Celzard et al., 2000).

REFERENCES

Aune, R.E., Hayashi, M., Nakajima, K., Seetharaman, S., 2002. Thermophysical properties of silicate slags. Journal of Metals (JOM) 11, 62–69.

Bird, R.B., Stewart, W.E., Lightfoot, E.N., 2005. Transport Phenomena, second edition. John Wiley & Sons, 898 pp.

Brandtzæg, S.R., 1985. Structural changes during calcinations of coke and anthracite. Doctoral Thesis. University of Trondheim, Norway, No. 45, 200 pp.

Brown, M.E., Dollimore, D., Galway, A.K., 1980. Reactions in solid state. In: Bamford, C.H., Tipper, C.F. (Editors), Comprehensive Chemical Kinetics, volume 22. Amsterdam, pp. 340.

Brown, M.E., 1989. Introduction to Thermal Analysis. Techniques and Applications. Chapman & Hall, London, 266 pp.

Celzard, A., Mareche, J.F., Payot, F., Begin, D., Furdin, G., 2000. Electrical conductivity of anthracites as a function of heat treatment temperature. Carbon 38, 1207–1215.

Dinsdale, A., 1991. SGTE data for pure elements. CALPHAD 15, 317–425.

Dyre, J.C., 1986. A phenomenological model for the Meyer-Neldel rule. Journal of Physics C: Solid State Physics 19, 5655–5664.

Flammersheim, H.J., Opfermann, J., 1999. Formal kinetic evaluation of reactions with partial diffusion control. Thermochemical Acta 337, 141–148.

Gasik, M.I., Gavrilov, V.A., 2001. Silicothermy of manganese. System Technologies, Dnipropetrovsk, 512 pp.

Gasik, M.I., Lyakishev, N.P., Gasik, M.M., 2009. Physical chemistry and technology of ferroalloys [in Ukrainian]. Sistemnye Tehnologii, Dnipropetrovsk, 494 pp.

Gasik, M.M., 2001. Reduction processes kinetics and experimental methods. In: Proceedings Seminaron Solid State Red-ox Reactions. POHTO, Finland, Oulu, 40 pp.

Gasik, M.M., Gasik, M.I., 2010. Multi-variation analysis and optimisation of electrical conductivity of MnO-CaO-SiO_2 slags. Proceedings of the 12th International Ferroalloys Congress. Editor: A. Vartiainen. Helsinki, Finland, 537–545.

Gasik, M.M., Gasik, M.I., Urazlina Yu, O., Kutuzov, S.V., 2010. Modelling and optimisation of anthracite treatment in an electrocalcinator. Proceedings of the 12th International Ferroalloys Congress., Editor: A. Vartiainen. Helsinki, Finland, 339–347.

Hauke, G., Hughes, T.J.R., 1994. A unified approach to compressible and incompressible flows. Computer Methods in Applied Mechanics and Engineering 113, 389–395.

Hillert, M., 1998. Phase Equilibria, Phase Diagrams and Phase Transformations: Their Thermodynamic Basis. Cambridge University Press, Cambridge, UK, 540 pp.

Incropera, F., DeWitt, D.P., 1996. Fundamentals of Heat and Mass Transfer, fourth edition. John Wiley & Sons, NY, 834 pp.

Kondratiev, A., Jak, E., Hayes, P.C., 2002. Predicting slag viscosities in metallurgical systems. Journal of Metals (JOM) 11, 41–45.

Kubaschewski, O., Alcock, C.B., 1979. Metallurgical Thermochemistry, fifth edition. Pergamon Press, Oxford, UK, 462 pp.

Lupis, C.H.P., 1983. Chemical Thermodynamics of Materials. North-Holland, New York, 602 pp.

McCabe, W.L., Smith, J.C., 1976. Unit Operations of Chemical Engineering, third edition. McGraw-Hill, NY, 1028 pp.

Meyer, W., Neldel, H., 1937. Über die Beziehungen zwischen der Energiekonstanten ε under der Mengenkonstanten α in der Leitwerts-Temperaturformel bei oxydischen Halbleitern. [Upon dependence of the energy constant of quantity constant in temperature-dependent conductivity of oxide semiconductors] Zeitschrift für Technische Physik [J Techn. Physics] 18, 588–593.

Ostrik, P.N., Gasik, M.M., 1993. Hydrogen reduction of MoO_3-Fe mixes studied by stepwise differential isothermal analysis. Journal of Thermal Analysis 40, 313–319.

Pelton, A.D., 2001. Thermodynamics and phase diagrams of materials. In: Kostorz (Ed.), Phase Transformations in Metals. G. Wiley-VCH, Weinheim, 724 pp.

Pelton, A.D., 1988. A database and sublattice model for molten salt solutions. CALPHAD 12, 127–142.

Saunders, N., Miodownik, A.P., 1998. CALPHAD, Calculation of Phase Diagrams, A Comprehensive Guide. Pergamon Materials Series, Oxford, 465 pp.

Seetharaman, S., Sichen, D., 1994. Estimation of the viscosities of binary metallic melts using Gibbs energies of mixing. Metallurgical and Materials Transactions 25B, 589–595.

Segers, L., Fontana, A., Winand, R., 1978. Conductivities electriques de melanges de silicates fondus du systeme CaO-SiO_2-MnO. Electrochimica Acta 23, 1281–1286.

Sridhar, S., 2002. Estimation models for molten slag and alloy viscosities. Journal of Metals 11, 46–50.

Swalin, R.A., 1956. Correlation between frequency factor and activation energy for solute diffusion. Journal of Applied Physics 27, 554–555.

Themelis, N.J., 1995. Transport and Chemical Rate Phenomena. Gordon & Breach Publishers, Basel, 370 pp.

VDI - Verein Deutscher Ingenieure, 1993. Heat Atlas. VDI-Verlag GmbH, Düsseldorf.

Wesselingh, J.A., Krishna, R., 2000. Mass Transfer in Multicomponent Mixtures. Delft University Press, Delft, 332 pp.

Zubov, V.L., Gasik, M.I., 2002. Electrometallurgy of ferrosilicon. System Technologies, Dnipropterovsk, 704 pp.

Zubov, V.L., Ovcharuk, A.N., Gasik, M.I., 2001. Physico-chemical properties, structural characteristics of carbon reductants and their use in smelting ferrosilicon. System Technologies, Dnipropetrovsk, 144 pp.